Mineralium Deposita
https://doi.org/10.1007/s00126-025-01355-x

ARTICLE

The gradual shift from forearc basalt-like to boninite-like magmatism during intra-oceanic subduction-initiation recorded by ophiolitic chromite deposits from Cuba

D. Domínguez-Carretero[1] · J. A. Proenza[1] · N. Pujol-Solà[2] · F. Gervilla[2] · C. Villanova-de-Benavent[1] · V. Colás[3] · K. Núñez-Cambra[4] · E. Piñero-Pérez[5] · A. Garcia-Casco[2]

Received: 8 August 2024 / Accepted: 24 February 2025

Abstract

Cuba contains the largest number of ophiolitic chromite deposits throughout the Americas. Most of these deposits are found within the mantle section of the Eastern Cuba and Camagüey ophiolitic massifs, which contain four different chromite mining districts (Camagüey, Mayarí, Sagua de Tánamo, and Moa-Baracoa). In addition to their potential as economic resources, chromite deposits are also excellent petrogenetic indicators to interpret the nature of ancient upper mantle, processes of melt formation in the mantle, and large-scale geodynamic processes. In this sense, major and trace elements of unaltered Cr-spinel cores together with chromitite whole-rock PGE composition reveal that high-Al Camagüey and Moa-Baracoa chromite districts were formed in equilibrium with forearc basalts (FAB)-like magmas during the incipient intra-oceanic subduction of the proto-Caribbean lithosphere underneath the Caribbean lithosphere, in a subduction-initiation process. Conversely, the high-Cr Mayarí chromite district was formed in equilibrium with more hydrated melts of boninitic affinity, typical of a more advanced stage of the subduction-initiation process. Nonetheless, the shift from FAB-like to boninite-like magmatism in an intra-oceanic subduction is gradual. This progressive change is well-recorded in the Sagua de Tánamo district that contains both high-Al and high-Cr chromitites. Thus, the studied ophiolitic chromitites allow tracing the complete magmatic evolution of an intra-oceanic subduction-initiation process. Furthermore, our data exhibits that accessory Cr-spinel composition of peridotites surrounding chromitites can be used as a prospecting indicator to anticipate the composition of ophiolitic chromitite bodies. Systematically, Cr-spinel from dunites associated with high-Al chromite deposits have lower Cr# values compared to the accessory Cr-spinel from the associated harzburgites. On the contrary, Cr-spinel from dunites of high-Cr chromite deposits show higher Cr# compared to the accessory Cr-spinel from the host harzburgites.

Keywords Ophiolitic chromitites · Platinum group elements (PGE) · Subduction-initiation · Forearc basalts · Boninites · Parental magmas

Editorial handling: B. Lehmann

✉ D. Domínguez-Carretero
ddominguezcarretero@ub.edu

[1] Departament de Mineralogia, Petrologia i Geologia Aplicada, Facultat de Ciències de la Terra, Universitat de Barcelona, Carrer Martí i Franquès, s/n, Barcelona 08028, Spain

[2] Departamento de Mineralogía y Petrología, Facultad de Ciencias, Universidad de Granada, Avda. Fuentenueva, s/n, Granada 18071, Spain

[3] Departamento de Ciencias de la Tierra, Universidad de Zaragoza, Pedro Cerbuna 12, Zaragoza 50009, Spain

[4] Instituto de Geología y Paleontología de Cuba, Línea del Ferrocarril s/n, Vía Blanca, San Miguel del Padrón, Habana 10200, Cuba

[5] Empresa Geominera Camagüey, Carretera Central Km 5 ½, Camagüey, Cuba

Published online: 07 March 2025

Introduction

Chromium has a wide range of applications in the metallurgy and chemical industries and plays a critical role in the production of stainless steel (USGS 2024). Chromium, in the form of Cr-spinel, is extracted from layered igneous complexes containing stratiform chromitite deposits (e.g. Bushveld Complex, South Africa) or from chromitite deposits found within the mantle section of ophiolitic sequences (e.g. Kempirsai, Kazakhstan). In 2023, Cr reserves were divided equally between both typologies and its production was divided approximately in a 40:60 ratio between ophiolitic chromitites and stratiform chromitites, respectively (USGS 2024). Besides, Cr has been catalogued as a critical metal by some national agencies from countries like the U.S.A. (Burton 2022), Japan (Nakano 2021), or India (Gupta et al. 2016), due to the high geographical concentration of the reserves of this metal (>95% are found in South Africa and Kazakhstan; USGS 2024). In this context, Cuba hosts the largest number of ophiolitic chromite deposits throughout the whole Caribbean region and the Americas (Proenza et al. 1999, 2001; Nelson et al. 2011). Cuban chromite deposits have had a protracted mining history that goes back to the 1840s (Thayer 1942). However, it was not until the beginning of the 20th century, due to the stimulus of the World War I high prices for metals, that the exploration and production of chromite deposits in Cuba started flourishing (Thayer 1942; Guild 1947). The finding and subsequent exploitation of new deposits continued throughout the century, especially since the 1960s with the creation of the Cuban Institute of Mineral Resources that closely collaborated with geological surveys from the Soviet Union and other eastern European countries (e.g. Semionov 1968).

Cuban chromite deposits are found within the mantle sequence of the Cuban ophiolitic belt, which extends discontinuously throughout the totality of the island along ca. 1000 km (Lewis et al. 2006; Iturralde-Vinent et al. 2016). Chromite deposits were originally grouped into four different mining regions, according to their geographic situation (Thayer 1942), which from NW to SE were: (i) Matanzas, (ii) Camagüey, (iii) Holguín, and (iv) Eastern Cuba. The Eastern Cuba and Camagüey districts are the largest and yield the highest numbers in terms of chromite resources. These districts are hosted respectively by the Eastern Cuba and Camagüey ophiolitic massifs, which are the two largest ophiolite massifs of the island (Fig. 1) and together contain over 500 deposits and occurrences of both high-Cr and high-Al chromitites (Murashko and Lavandero 1989; Proenza et al. 1999; Henares et al. 2010; Nelson et al. 2011). Nowadays, many chromite deposits from the Camagüey district (Flint et al. 1948; Henares et al. 2010) are under production and exploration campaigns exist in the area. In the Eastern Cuba district, production is more intermittent because the largest deposits have already been extensively mined in the past (e.g. Proenza et al. 1999, 2001, 2018; Gervilla et al. 2005; González-Jiménez et al. 2011).

In addition to their economic relevance, Cr-spinel are important petrogenetic indicators, as they decipher the nature of ancient upper mantle, processes of melt formation in the mantle, and large scale geodynamic processes (e.g. Melcher et al. 1997; Arai 1997; Proenza et al. 1999, 2018; Gervilla et al. 2005; Rollinson et al. 2008; Pagé and Barnes 2009; Zaccarini et al. 2011; González-Jiménez et al. 2011, 2014; Uysal et al. 2018; Chen et al. 2019; Pujol-Solà et al. 2021). Chromitites from Cuba have been used to understand the magmatic and geodynamic evolution of the Caribbean margin during the Cretaceous (Proenza et al. 1999, 2018; Gervilla et al. 2005). These investigations concluded that high-Cr chromitites originated from boninitic melts formed during subduction-initiation, whereas high-Al chromitites crystallized in equilibrium with mid-ocean ridge basalt-like (MORB) melts associated to back-arc basins (Proenza et al. 1999; Zhou et al. 2001a; Gervilla et al. 2005). A significant problem with this interpretation is denoted by the Sagua de Tánamo district, in eastern Cuba (Fig. 1c). This district contains both high-Cr and high-Al chromitites (González-Jiménez et al. 2011), and its origin is difficult to reconcile with contrasted tectonic scenarios such as forearc and back-arc. It must be noted that these interpretations were proposed before the discovery of forearc basalt (FAB) melts (Reagan et al. 2010; Shervais et al. 2019), which are similar to MORB melts. FAB melts open the possibility of explaining the formation of high-Al chromitites during the early stages of subduction-initiation (e.g. Uysal et al. 2018; Chen et al. 2019; Zhang et al. 2020; Pujol-Solà et al. 2021) without the necessity of invoking a back-arc setting for their formation.

This contribution evaluates the petrogenesis of chromitites from the Camagüey and Eastern Cuba chromite districts together with their associated dunites and harzburgites. A detailed mineralogical characterization of the chromitites and the mineral inclusions within Cr-spinel, in addition to a large dataset of Cr-spinel major, minor and trace elements composition and platinum-group elements (PGE) chromitites whole-rock composition allows addressing the formation of the different types of chromitites and their parental melts. Finally, all this information is combined to constrain the geodynamic setting in which these chromitites originated within a subduction-initiation scenario.

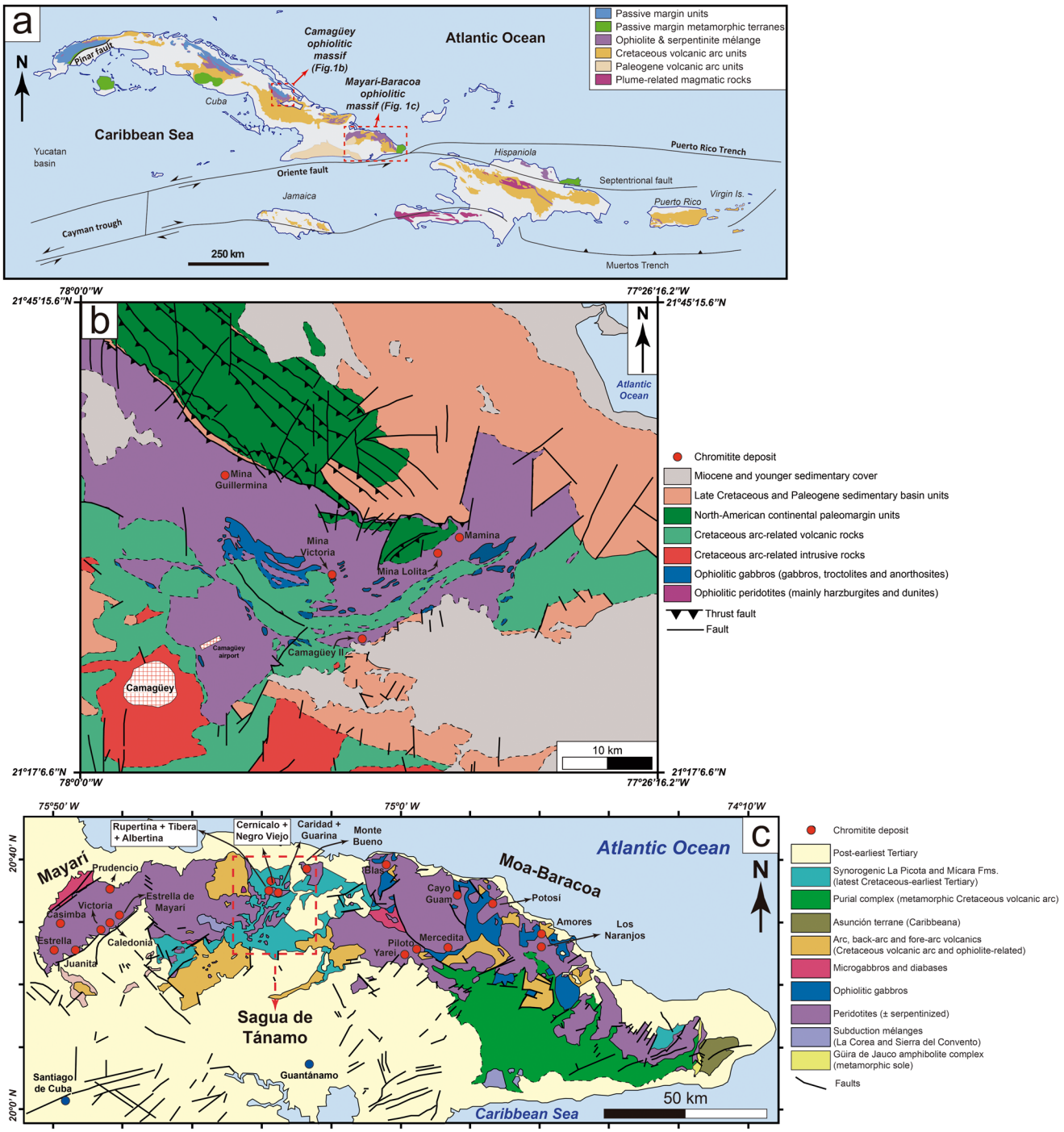

Fig. 1 (**a**) Simplified geological map of the Greater Antilles (modified from Wilson et al. 2021). (**b**) Geological map of the Camagüey ophiolitic massif (modified from Instituto de Geología y Paleontología 1985). (**c**) Geological map of the Mayarí-Baracoa Ophiolite Belt (after Pushcharovsky 1988). Maps in (**b**) and (**c**) include the location of the studied chromite deposits

Geological setting

Cuban ophiolitic belt

The Cuban ophiolitic belt crops out discontinuously for more than 1000 km along the island (Fig. 1a). The belt consists of discrete and variously sized mafic and ultramafic bodies alongside serpentinite-matrix mélanges locally containing subduction-related high-pressure blocks (Iturralde-Vinent 1996; García-Casco et al. 2006; Lewis et al. 2006; Iturralde-Vinent et al. 2016). This belt represents slices of oceanic lithosphere obducted onto the North American plate

due to the collision between the Caribbean volcanic arc and the passive continental margins of the Bahamas and the Maya block between the Late Cretaceous to Mid Eocene (Iturralde-Vinent 1996; García-Casco et al. 2008; Iturralde-Vinent et al. 2016). The ophiolite assemblages include variably serpentinized ultramafic and mafic rocks (harzburgites, dunites, wehrlites, peridotites with plagioclase and clinopyroxene, gabbro sills and dikes) from the mantle and the Moho Transition Zone (MTZ), along with oceanic crustal rocks such as layered and isotropic gabbros, dikes, and volcanic and sedimentary rocks. Petrological, geochemical, and geochronological analyses suggest that the Cuban ophiolites predominantly originated in a suprasubduction zone (SSZ) setting (Proenza et al. 1999; Marchesi et al. 2006; Lázaro et al. 2016; Iturralde-Vinent et al. 2016; Farré-de-Pablo et al. 2020; Rui et al. 2021).

The Camagüey ophiolitic Massif

The region of Camagüey is situated in central-eastern Cuba, ca. 500 km to the east of Havana. The Camagüey ophiolitic massif has an extension of ~1200 km^2 with an arc-shaped morphology and a broad zone dominated by partially altered mafic and ultramafic rocks (Fig. 1b). The ophiolite is subdivided into two superimposed ophiolite nappes that contain mantle peridotites, lower crust gabbroic rocks, subvolcanic mafic rocks, basalts, and cherts (Iturralde-Vinent 1996). The mantle section of the ophiolitic sequence is made up of mostly harzburgites, and minor dunites, websterites, and lherzolites. Troctolite, gabbro, and anorthosite bodies are abundant in the upper parts of the mantle and the lower sections of the oceanic crust, in the MTZ (ESM 1 Fig. 1a). Albian-Cenomanian basaltic rocks, cherts, radiolarites, and limestones form the upper part of the ophiolitic sequence (Henares et al. 2010). The whole sequence thrusts towards the NE upon rocks that belonged to the Bahamas Platform of the North American Plate (van Hinsbergen et al. 2009).

The mantle section of the Camagüey ophiolitic massif contains an important refractory grade (high-Al) chromite district with over 1 Mt in chromite reserves (Nelson et al. 2011) and more than 340 chromite occurrences and deposits (Flint et al. 1948; González-Pontón 2009; Henares et al. 2010). The chromite ore bodies in Camagüey are found within the MTZ and are typically hosted by dunite envelopes within harzburgite (ESM 1 Fig. 1a). The chromitite bodies are usually massive (Fig. 2a), except for Mina Guillermina mine, where chromitites are nodular. Chromitites are all parallel to the foliation of the enclosing peridotites and oftentimes they are crosscut by gabbro or troctolite dikes (Flint et al. 1948; González-Pontón 2009; Fig. 2a). The largest deposit in the district is the Camagüey-II mine (Fig. 2a), whose chromite reserves exceed 700,000 tons, followed by Victoria, Mamina, and Lolita mines, which have reserves between 150,000 and 90,000 tons (Henares et al. 2010).

The Mayarí-Baracoa ophiolitic belt

In eastern Cuba, ophiolitic bodies are grouped into the Mayarí-Baracoa Ophiolite Belt (MBOB; Fig. 1c). The MBOB is tectonically emplaced on subduction-related metamorphic mélanges that contain high-pressure blocks (e.g. Sierra del Convento mélange; García-Casco et al. 2006, 2008) and the La Corea Melánge (Blanco-Quintero et al. 2011). During Late Cretaceous to Early Paleocene

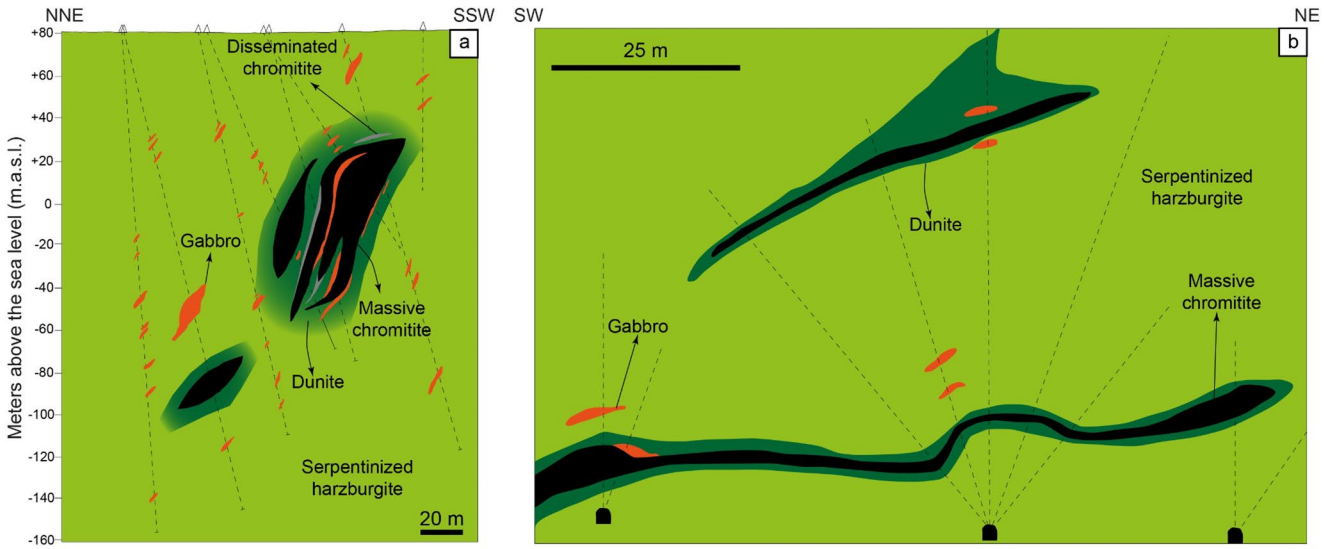

Fig. 2 (**a**) Camagüey-II (Camagüey district) mine vertical cross-section interpreted from eight surface drillholes. Data courtesy of Empresa Geominera Camagüey (Cuba). (**b**) Mercedita (Moa-Baracoa district) mine vertical cross-section made from nine holes drilled upward from the roof of the mine's galleries. Data courtesy of Empresa Unidas Geólogo Minera Moa (Cuba)

(Iturralde-Vinent et al. 2006), the ophiolitic belt and their associated metamorphic complexes were accreted and thrusted over Cretaceous volcanic arc complexes (Lázaro et al. 2016), with diverse geochemical signatures including tholeiitic, boninitic, and calc-alkaline (Proenza et al. 2006; Marchesi et al. 2007).

The MBOB is composed of two allochthonous massifs (Proenza et al. 1999; Marchesi et al. 2006): the Mayarí-Cristal to the west and the Moa-Baracoa to the east (Fig. 1c). The Mayarí-Cristal massif (Fig. 1c, ESM 1 Fig. 1b) is formed by highly serpentinized harzburgite tectonites (5 km thick), hosting minor dunites, both crosscut by several generations of websterite and pyroxenite dikes formed from melts with boninitic affinity (Proenza et al. 1999; Gervilla et al. 2005; Marchesi et al. 2006). The ultramafic rocks overthrust a crustal unit consisting of gabbros, microgabbros, and abundant diabase dikes (Proenza et al. 1999; Marchesi et al. 2006, 2007). The easternmost part of the massif (Sagua de Tánamo region; ESM 1 Fig. 1c) is composed of highly serpentinized mantle tectonites (harzburgites and dunites), which are thrusted over the La Corea mélange and the Late Cretaceous arc-related Santo Domingo Formation volcanic rocks (Iturralde-Vinent et al. 2006; Proenza et al. 2006; Marchesi et al. 2006, 2007; Blanco-Quintero et al. 2011). The tectonic history of the Sagua de Tánamo region is complex and peridotites form thrust slices that locally appear interbedded within the mélange zone and volcanic arc rocks (Iturralde-Vinent et al. 2006). The Moa-Baracoa massif (ESM 1 Fig. 1d) consists of 2.2 km thick mantle tectonites, mainly harzburgites with minor dunites, a very well-preserved MTZ about 0.5 km thick, layered gabbros, and mafic volcanic rocks (Marchesi et al. 2006). Towards the upper parts of the MTZ there are abundant dunite and gabbro sills concordant to the foliation of the harzburgitic host, as well as discordant dikes of wehrlites, troctolites, olivine gabbros, and pegmatitic gabbros (Guild 1947; Proenza et al. 1999; Marchesi et al. 2006). The peridotites and gabbros are in tectonic contact above the pillow basalts of the Morel Formation paleontologically dated at 88–91 Ma (Iturralde-Vinent et al. 2006).

The MBOB contains the largest chromite reserves in the Caribbean region, with chromite reserves over 6.5 Mt (Nelson et al. 2011). The Mayarí-Cristal massif contains ~ 40 metallurgical grade (high-Cr) chromite deposits, including the large deposits of Casimba and Caledonia, whose reserves exceed 200,000 tons each (Proenza et al. 1999). The chromitite ore bodies are located in dunite envelopes hosted in harzburgites (ESM 1 Fig. 1b). The chromitites are generally massive, even though banded (e.g. Estrella deposit) or even nodular chromitites (e.g. Caledonia mine) locally occur and are crosscut by pyroxenite dikes.

The Sagua de Tánamo chromite deposits are smaller in size, with a total of 35 deposits of either metallurgical or refractory grade (Murashko and Lavandero 1989; González-Jiménez et al. 2011). Chromitites form massive lenses of variable sizes (up to 40 m long, 20 m wide, 3 m thick; González-Jiménez et al. 2011) and are separated from the harzburgitic host by dunite envelopes (ESM 1 Fig. 1c). Some chromitites are crosscut by amphibole-bearing gabbros (González-Jiménez et al. 2011).

The Moa-Baracoa massif is the most important chromite district in eastern Cuba, containing more than 100 deposits of refractory grade chromite and reserves exceeding 6 Mt (Nelson et al. 2011). Mercedita is the largest deposit with reserves over 5 Mt (Fig. 2b), and other minor deposits, like Amores, Yarey, and Piloto contain more than 100,000 tons of chromite reserves (Proenza et al. 1999; Nelson et al. 2011). Additionally, Cayo Guam and Potosí deposits, extensively exploited in the past, have produced over 800,000 tons of chromite each (Proenza et al. 1999, 2001). As in the other chromite districts, the chromitites bodies are generally massive and have a dunite envelope that separates them from the harzburgite host (Fig. 2b and ESM 1 Fig. 1d). Chromitite bodies are all parallel to the foliation of the enclosing peridotites. Gabbro dikes, often crosscutting the chromitites bodies (Proenza et al. 1999; Pujol-Solà et al. 2020), and sills, scarcer and subparallel to the chromitites, are also found (Proenza et al. 1999). Less abundantly, nodular chromitites are also present in some areas of the Mercedita deposit.

Samples and analytical techniques

We studied representative samples of chromitites and associated dunites and harzburgites from chromite deposits from Camagüey ($n=5$), Mayarí ($n=7$), Sagua de Tánamo ($n=8$) and Moa-Baracoa ($n=8$) districts (Figs. 1 and 2). Polished thin sections from chromitites, dunites, and harzburgites were studied in detail by optical microscopy and scanning electron microscopy, using both a Quanta 200 FEI XTE325/D8395 scanning electron microscope (SEM) and a JEOL JSM-7100 field-emission SEM at the Scientific and Technological Centers of the Universitat de Barcelona (CCiTUB). Operating conditions were 15–20 kV accelerating voltage and 5 nA beam current.

Geochemical data were obtained by quantitative electron microprobe analyses (EMPA), laser ablation inductively coupled plasma mass spectrometry (LA-ICP-MS), and nickel sulfide fire assay with ICP-MS finish. The full dataset of EMPA results, including the methodology and detection limits, for Cr-spinel and silicate inclusions are presented in ESM 2. All LA-ICP-MS data, including the methodology,

element concentration, 2-sigma errors, detection limits and the tables with the repeated analysis of the two standards and their comparison with literature values are presented in ESM 3. Finally, all whole-rock PGE bulk composition results, including the methodology and detection limits, can be found in ESM 4.

Petrography

Chromitites and host peridotites

The chromitites from the studied districts predominantly display four distinctive types of textures: massive, banded, disseminated, and nodular (Fig. 3).

The most common texture is massive (Fig. 3a; Cr-spinel > 90 vol%), with subhedral Cr-spinel grains ranging from ~ 100 μm to ~ 3 mm in size (Fig. 3b). Cr-spinel is generally unaltered and exhibits abundant pull-apart fractures. Occasionally, Cr-spinel may appear brecciated, especially near veins crosscutting the chromitites. Interstitial silicates, such as serpentine, chlorite, and minor relic olivine, and Fe-Ni sulfides are found in between the Cr-spinel grains.

Toward the contact with the enclosing dunite, the massive texture usually grades to banded (Fig. 3c) and disseminated (Fig. 3e) with lower Cr-spinel vol% (~ 50 to 20 vol%). The Cr-spinel grains are anhedral to subhedral and display sizes from ~ 50 μm to ~ 1 mm (Fig. 3d and f). Pervasive pull-apart fracturing is also common, especially in the banded texture (Fig. 3d). The silicate matrix is mostly made of secondary minerals, mainly serpentine-group minerals and chlorite to a lesser extent. Small remnants of pristine olivine can still be found occasionally, and small amounts of Fe-Ni sulfides are also present within the matrix.

The least common textural type is represented by nodular chromitite (Fig. 3g). This type of chromitite consists of oval-shaped nodules of Cr-spinel with sizes up to 1–2 cm. The nodules are formed by aggregates of Cr-spinel grains (Fig. 3h), whose center is locally filled with serpentine, and in the case of high-Al chromite deposits such as in the Camagüey district, also small amounts of partially altered plagioclase. The Cr-spinel nodules appear to be more fractured towards their more external parts. The matrix within the nodules cores is mostly made of serpentine and minor amounts of chlorite. In the high-Al chromite districts, the matrix of nodular chromitites also contains altered plagioclase.

Dunites and harzburgites enclosing chromitites are usually strongly serpentinized (> 80 vol%) and contain minor chlorite. However, accessory Cr-spinel grains with sizes up to ~ 500 μm are well-preserved with unaltered cores. Magnetite is found as secondary mineral in the Cr-spinel rims. Cr-spinel grains in dunite are anhedral to subhedral, whereas in harzburgite they show subhedral or vermicular morphologies. Only in a few local areas, pristine primary silicates, mostly olivine and orthopyroxene and minor clinopyroxene remain unaltered. Olivine grains, with sizes up to 1–2 mm, display undulous extinction and are surrounded by serpentine. Orthopyroxene porphyroclasts in harzburgite have sizes of up to 5 mm, show undulous extinction, and are locally deformed displaying kink bands. Most orthopyroxene grains are bastitized and pseudomorphed by serpentine and minor chlorite. Minor clinopyroxene (~ 200 μm grains) is found in harzburgites, usually transformed to amphibole. Additionally, in the case of Camagüey and Moa-Baracoa peridotites, clinopyroxene only occurs as interstitial secondary phase or as exsolution lamellae in orthopyroxene.

Mineral inclusions in Cr-spinel

Mineral inclusions are found in different proportions in Cr-spinel grains of chromitites from the four studied chromitite districts (Fig. 4). Inclusions within Cr-spinel are especially abundant in chromitites from the Mayarí and Sagua de Tánamo districts, whereas those are scarcer in Moa-Baracoa and Camagüey chromitites.

In this section, we focus on mineral inclusions not visibly connected to cracks or fractures that may have possibly reworked their pristine nature, and consequently suggesting that they co-crystallized with the host Cr-spinel. Furthermore, most of these inclusions are distributed concentrically within their Cr-spinel host grains, pointing to their entrapment during primary Cr-spinel growth. The size of the inclusions is usually small (< 20 μm), however, some may have larger dimensions (up to 200 μm), and their shapes are mostly anhedral to subhedral. The main included minerals (Fig. 4) are magmatic anhydrous silicates, especially, olivine, clinopyroxene and minor orthopyroxene, locally partially altered to serpentine and/or chlorite. Magmatic hydrous silicates, such as amphibole or phlogopite are also abundant, especially in Mayarí and Sagua de Tánamo chromitites. Other minerals, such as oxides (rutile, baddeleyite), sulfides (Ni-Fe sulfides, laurite-erlichmanite), alloys (Os-Ir, Ru-Os-Ir-Fe-Ni), sulfarsenides (irarsite-ruarsite), and phosphates (apatite) are also present. The majority of the inclusions characterized are polyphasic, and only a few monomineralic inclusions are found, generally corresponding to magmatic anhydrous silicates, such as olivine or clinopyroxene, and magmatic sulfides, such as laurite-erlichmanite or Ni-sulfides. Additionally, in some deposits from Camagüey (Mina Guillermina) and Moa-Baracoa (Mercedita) districts, Cr-spinel has rutile needles (Fig. 4l) crystallographically oriented following the (111) plane of Cr-spinel.

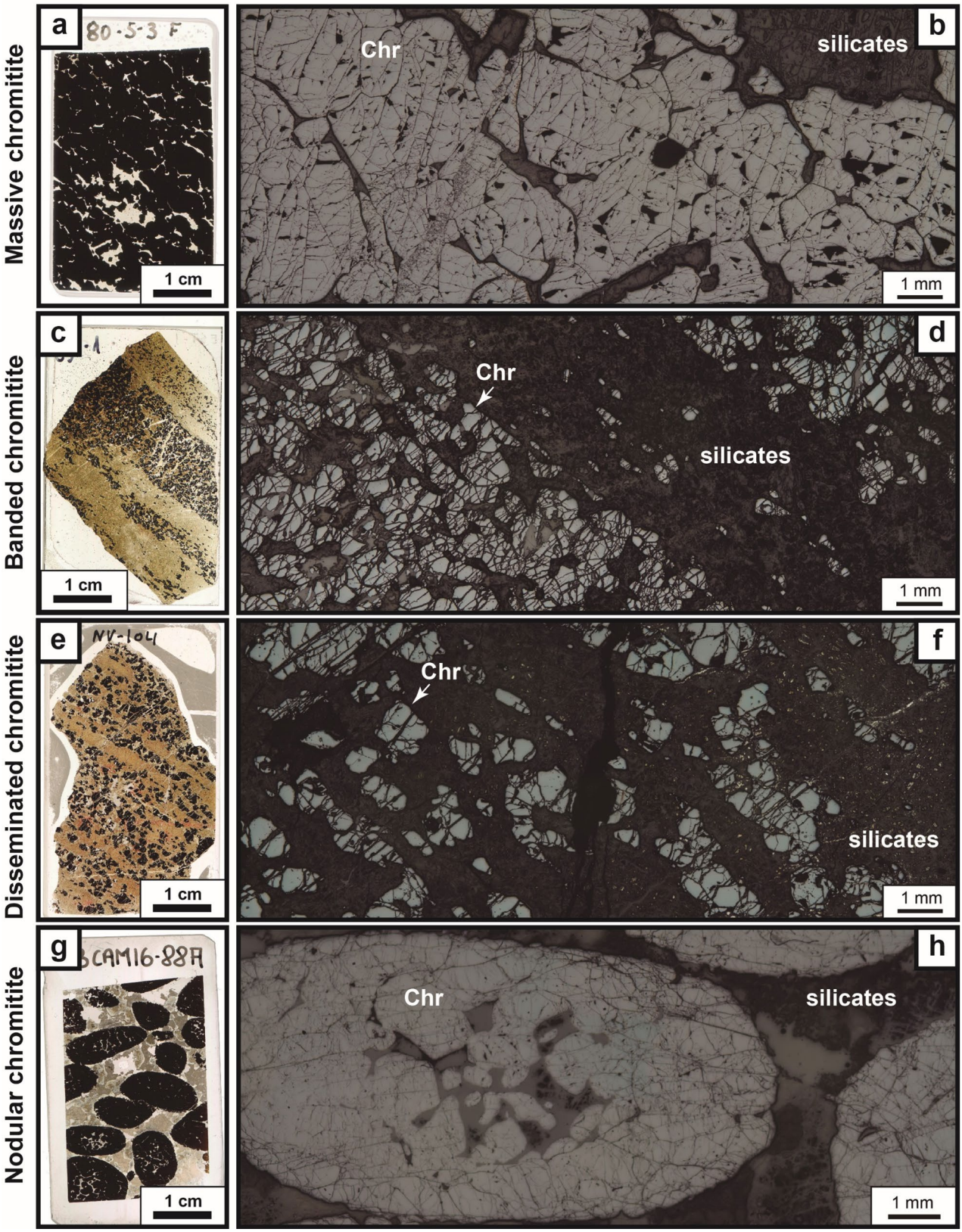

Fig. 3 Textures of chromitites. (**a-b**) Thin section of massive chromitite and a microphotograph panorama of it under reflected light (RL), from Mercedita deposit (Moa-Baracoa district). (**b**) Thin section of banded chromitite and a microphotograph panorama of it under RL from Estrella de Mayarí deposit (Mayarí district). (**c**) Thin section of disseminated chromitite and a microphotograph panorama of it under RL from Negro Viejo deposit (Sagua de Tánamo district). (**d**) Thin section of nodular chromitite and a microphotograph panorama of it under RL from Mina Guillermina deposit (Camagüey district). Abbreviations: Chr – Cr-spinel

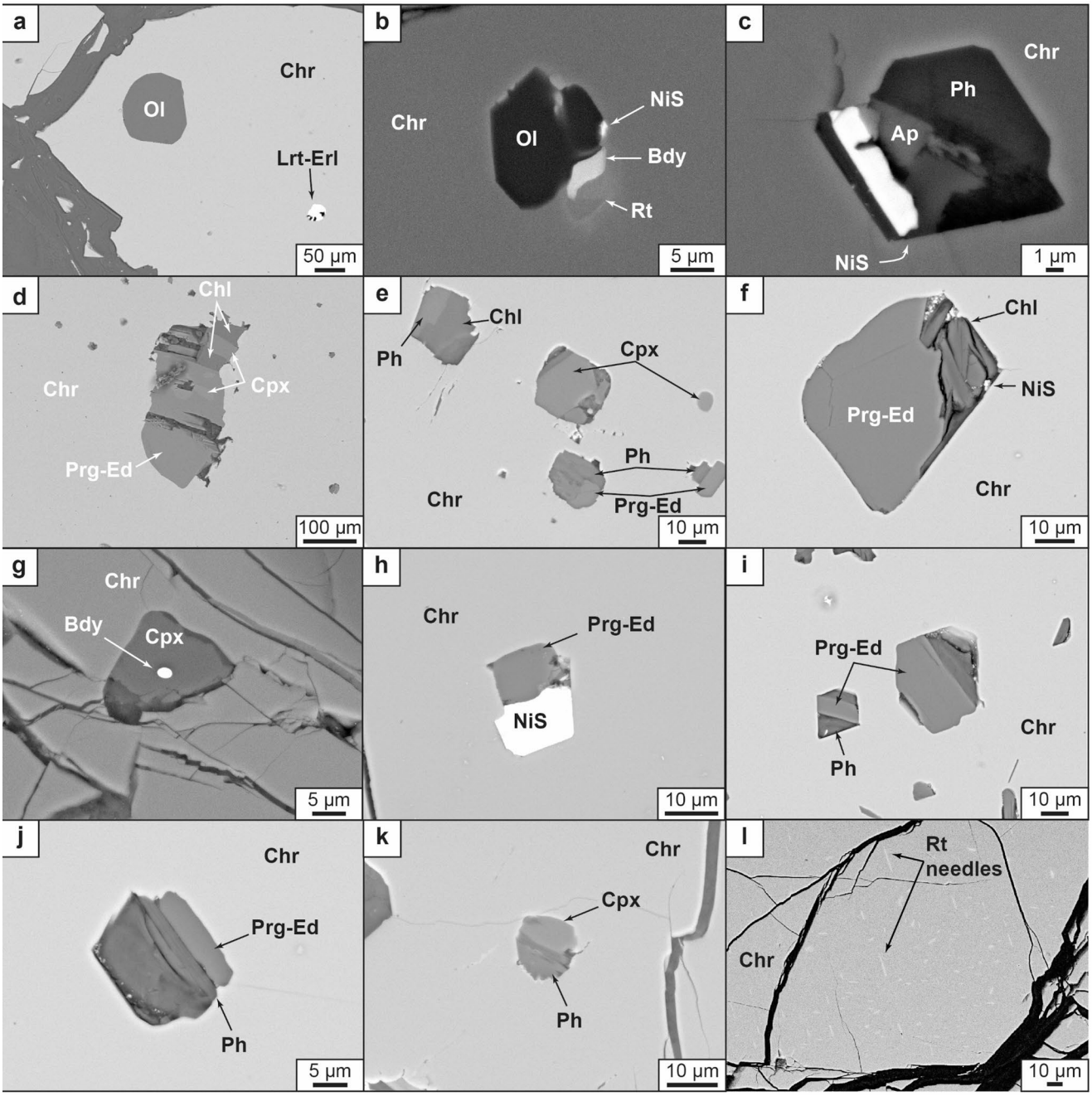

Fig. 4 Backscattered electron images of inclusions within Cr-spinel. (**a**) Rutile needles oriented according to the (111) plane of Cr-spinel. (**b**) Monomineralic inclusions of olivine and laurite-erlichmanite. (**c**) Polyphasic inclusion consisting of olivine, baddeleyite, rutile, and NiS. (**d**) Polyphasic inclusion of amphibole (pargasite-edenite), clinopyroxene (diopside), and secondary chlorite. (**e**) Polyphasic inclusions of phlogopite and amphibole (pargasite-edenite) or chlorite, and monophasic inclusions of clinopyroxene (diopside). (**f**) Polyphasic inclusion of amphibole (pargasite-edenite), secondary chlorite, and NiS. (**g**) Polyphasic inclusion of clinopyroxene (diopside) hosting a smaller inclusion of baddeleyite. (**h**) Polyphasic inclusion of amphibole (pargasite-edenite) and NiS. (**i**, **j**) Polyphasic inclusions of amphibole (pargasite-edenite) and phlogopite. (**k**) Polyphasic inclusion of clinopyroxene (diopside) and phlogopite. (**l**) Polyphasic inclusion of phlogopite, NiS and apatite. Abbreviations: Chr – Cr-spinel; Rt – Rutile; Ol – Olivine; Lrt-Erl – Laurite-Erlichmanite; Bdy – Baddeleyite; Prg-Ed – Pargasite-Edenite; Cpx – Clinopyroxene; Chl – Chlorite; Phl – Phlogopite; Ap – Apatite

Mineral chemistry of Cr-spinel (major, minor, and trace elements)

Cr-spinel mineral chemistry was obtained from primary unaltered Cr-spinel cores (median Fe^{3+}# [Fe^{3+}/(Fe^{3+}+Cr+Al)] below 0.1) from chromitites (Figs. 5 and 6 and ESM 1 Figs. 2, 3 and 4) and their host dunites and harzburgites (Figs. 5 and 6 and ESM 1 Fig. 2, ESM 2 and 3). The minimum, maximum and median values of Cr-spinel from chromitites, dunites and harzburgites of each district is found in Table 1. According to the Cr# [Cr/(Cr+Al)] of the Cr-spinel in chromitites, the different chromite deposits and districts will be hereafter classified as high-Cr (Cr# ≥ 0.60) and high-Al (Cr# < 0.60), following the usual dual classification used by most authors (i.e. Arai 1997; Proenza et al. 1999; Arai and Miura 2016; Zhu and Zhu 2020).

Camagüey district

Cr-spinel from chromitites

The Camagüey chromitites (n=169; Figs. 5a and 6a and ESM 1 Fig. 2a) are classified as high-Al, with Cr# ranging between 0.40 and 0.53 (median of 0.44) and Mg# [Mg/(Mg+Fe^{2+})] between 0.60 and 0.93 (median of 0.75). Their minor and trace element composition (n=34; ESM 1 Fig. 3) shows 831–1353 ppm V (median of 962 ppm), 1–10 ppm Sc (median of 4 ppm), 38–61 ppm Ga (median of 53 ppm), 453–3792 ppm Ti (median of 1514 ppm), 1032–1771 ppm Ni (median of 1489 ppm), 380–1201 ppm Zn (median of 524 ppm), 164–394 ppm Co (median of 197 ppm), and 873–1643 ppm Mn (median of 1191 ppm).

Cr-spinel from Dunites and Harzburgites

Major element composition of Cr-spinel (n=42; Figs. 5a and 6a and ESM 1 Fig. 2a) from Camagüey dunites have Cr# ranging from 0.36 to 0.47 (median of 0.43), and Mg# from 0.47 to 0.57 (median of 0.53). On the other hand, major element composition of Cr-spinel (n=94; Figs. 5a and 6a and ESM 1 Fig. 2a) from Camagüey harzburgites has Cr# ranging from 0.42 to 0.59 (median of 0.56), and Mg# from 0.44 to 0.62 (median of 0.53).

Mayarí district

Cr-spinel from chromitites

The Mayarí chromitites (n=256; Figs. 5b and 6b and ESM 1 Fig. 2b) are classified as high-Cr, with Cr# ranging from

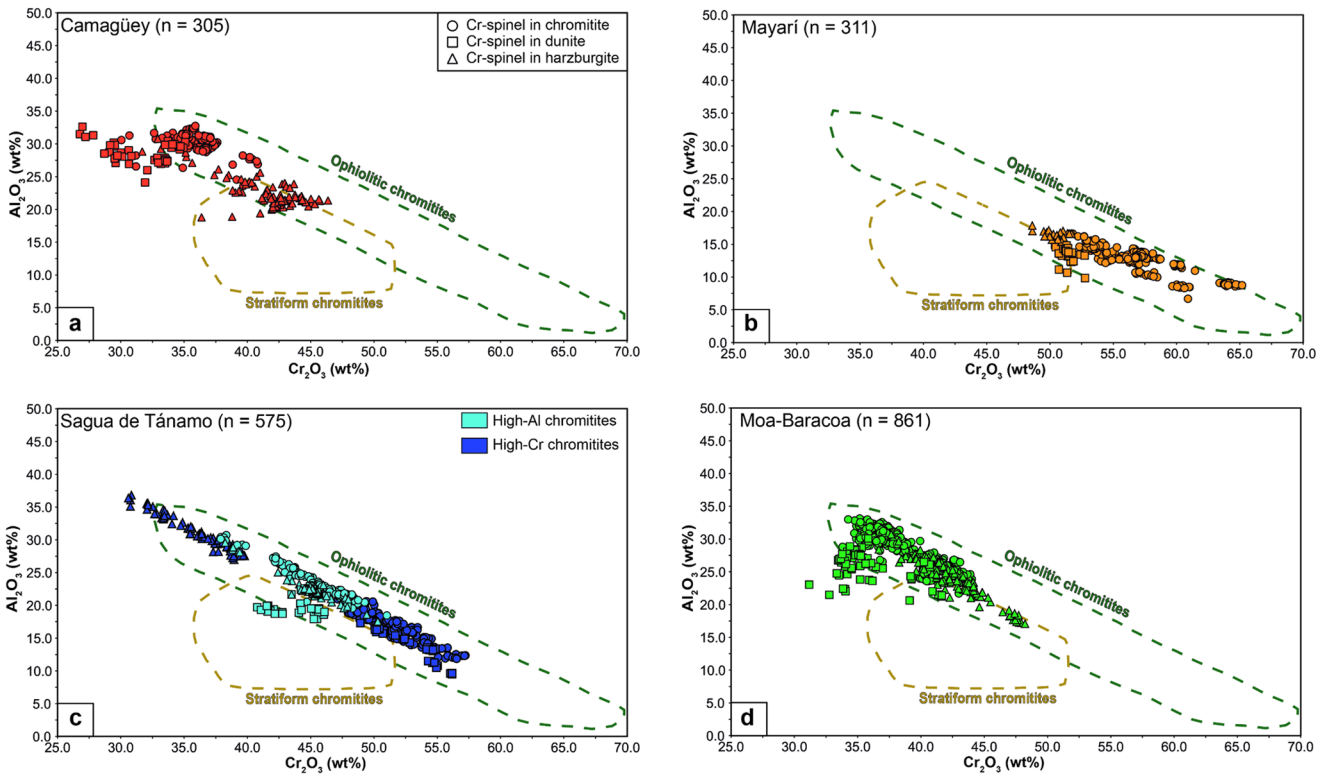

Fig. 5 Composition of Cr-spinel from chromitites and surrounding dunites and harzburgites from the four studied districts in a Cr_2O_3 (wt%) vs. Al_2O_3 (wt%) diagram. (**a**) Camagüey, (**b**) Mayarí, (**c**) Sagua de Tánamo, (**d**) Moa-Baracoa. Data sources for Cr-spinel of different tectonic settings are compiled from Bonavia et al. (1993), Kamenetsky et al. (2001), Proenza et al. (2007), and González-Jiménez et al. (2015)

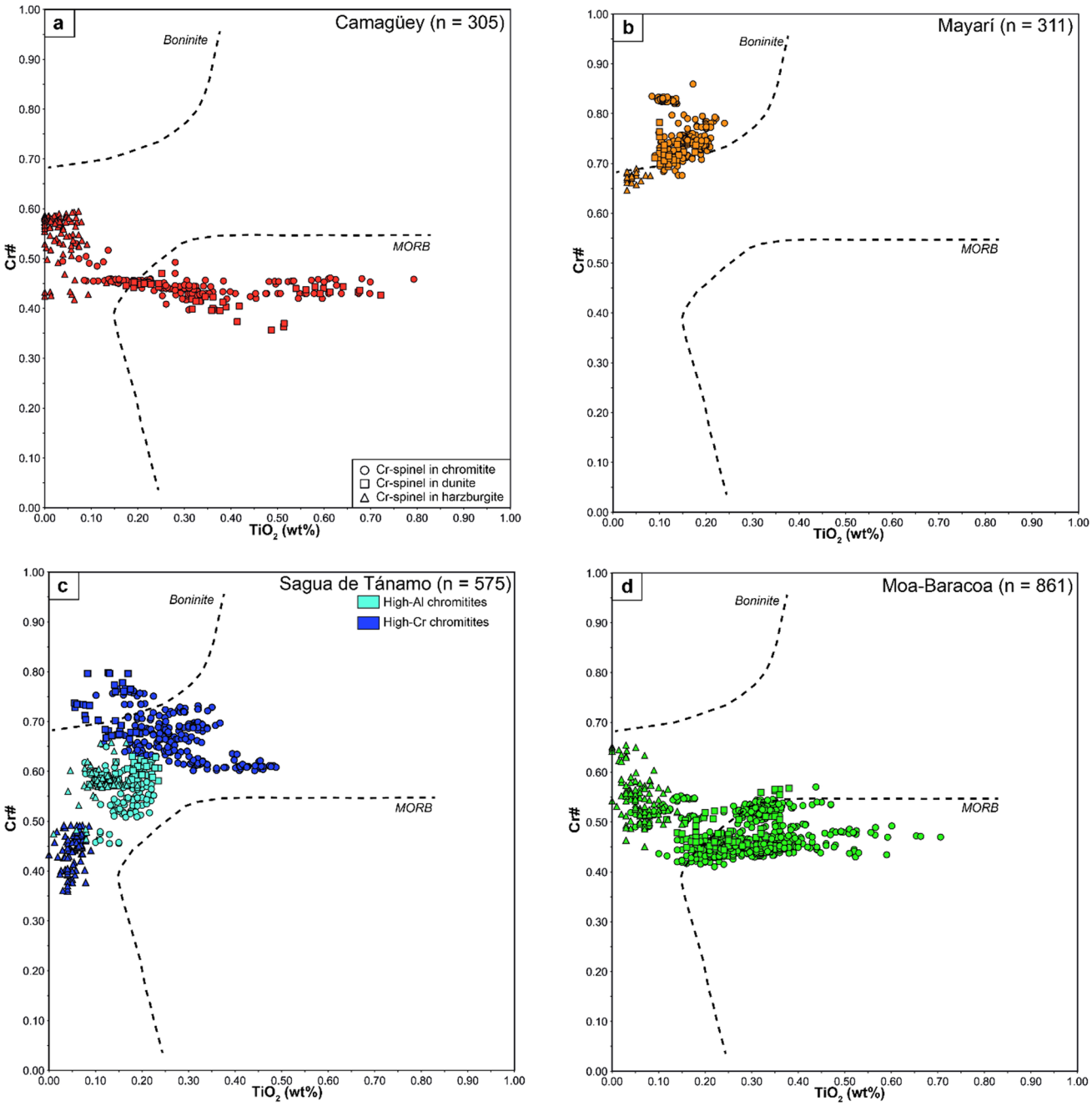

Fig. 6 Composition of Cr-spinel from chromitites and surrounding dunites and harzburgites from the four studied districts in a TiO_2 (wt%) vs. Cr# diagram. (**a**) Camagüey, (**b**) Mayarí, (**c**) Sagua de Tánamo, (**d**) Moa-Baracoa. Data for accessory Cr-spinel in boninites and MORB are from Arai (1992)

0.68 to 0.86 (median of 0.74) and Mg# from 0.51 to 0.78 (median of 0.67). Their minor and trace element compositions ($n=63$; ESM 1 Fig. 3) show contents of: 394–1490 ppm V (median of 783 ppm), 4–15 ppm Sc (median of 6 ppm), 19–32 ppm Ga (median of 25 ppm), 602–1050 ppm Ti (median of 757 ppm), 496–1152 ppm Ni (median of 785 ppm), 363–842 ppm Zn (median of 579 ppm), 233–383 ppm Co (median of 276 ppm) and 1176–1927 ppm Mn (median of 1565 ppm).

Cr-spinel from Dunites and Harzburgites

Major element composition of Cr-spinel ($n=31$; Figs. 5b and 6b and ESM 1 Fig. 2b) from Mayarí dunites have Cr# that ranges from 0.69 to 0.78 (median of 0.72) and Mg#

Table 1 Cr-spinel composition (minimum, maximum and median values) from chromitites, Dunites and Harzburgites of the four studied chromite districts

District	Rock	Cr_2O_3	Al_2O_3	TiO_2	FeOt	Cr#	Mg#
Camagüey	Chromitite	30.1–40.8 (36.5)	23.6–32.8 (30.4)	0.04–0.79 (0.30)	12.5–22.2 (14.3)	0.40–0.53 (0.44)	0.60–0.93 (0.75)
	Dunite	26.8–35.1 (32.8)	24.1–32.6 (28.4)	0.17–0.72 (0.35)	21.2–29.8 (25.4)	0.36–0.47 (0.43)	0.47–0.57 (0.53)
	Harzburgite	31.7–46.4 (42.1)	18.8–30.8 (21.9)	b.l.d.-0.13 (0.05)	19.6–28.3 (21.9)	0.42–0.59 (0.56)	0.44–0.62 (0.53)
Mayarí	Chromitite	51.6–65.2 (56.7)	6.7–16.6 (13.0)	0.08–0.24 (0.15)	12.6–21.3 (15.1)	0.68–0.86 (0.74)	0.51–0.78 (0.67)
	Dunite	50.4–52.8 (51.4)	9.8–14.9 (13.5)	0.09–0.18 (0.11)	21.3–26.0 (22.1)	0.69–0.78 (0.72)	0.42–0.55 (0.51)
	Harzburgite	48.6–51.7 (50.6)	15.4–17.9 (16.6)	0.03–0.08 (0.04)	19.4–21.5 (20.7)	0.65–0.69 (0.67)	0.48–0.54 (0.51)
Sagua de Tánamo	Chromitite	37.9–57.2 (48.4)	11.9–30.7 (20.2)	0.08–0.49 (0.22)	12.2–22.2 (16.2)	0.46–0.76 (0.62)	0.45–0.74 (0.65)
	Dunite	40.8–56.2 (45.5)	9.5–22.9 (19.0)	0.06–0.24 (0.15)	18.1–29.1 (21.6)	0.57–0.80 (0.61)	0.35–0.61 (0.51)
	Harzburgite	30.6–50.4 (38.6)	17.6–36.8 (28.7)	b.l.d.-0.19 (0.07)	15.8–21.7 (17.6)	0.36–0.66 (0.47)	0.47–0.67 (0.62)
Moa-Baracoa	Chromitite	33.8–44.0 (37.8)	21.7–33.1 (29.7)	0.04–0.71 (0.31)	12.7–24.8 (14.9)	0.41–0.57 (0.46)	0.44–0.81 (0.71)
	Dunite	31.2–41.7 (35.2)	20.6–30.1 (26.2)	0.12–0.38 (0.24)	18.4–32.3 (23.1)	0.44–0.57 (0.48)	0.50–0.67 (0.59)
	Harzburgite	36.7–48.2 (42.3)	17.1–30.8 (23.5)	b.l.d.-0.15 (0.06)	17.1–24.6 (20.1)	0.45–0.65 (0.55)	0.39–0.68 (0.55)

from 0.42 to 0.55 (median of 0.51). The major element composition of Cr-spinel ($n=42$; Figs. 5b and 6b and ESM 1 Fig. 2b) from Mayarí harzburgites have Cr# ranging from 0.65 to 0.69 (median of 0.67) and Mg# from 0.48 to 0.54 (median of 0.51).

Sagua de Tánamo district

Cr-spinel from chromitites

The composition of Cr-spinel from Sagua de Tánamo chromitites ($n=351$; Figs. 5c and 6c and ESM 1 Fig. 2c) is very contrasted with Cr# varying between 0.46 and 0.76 (median of 0.62) and the Mg# from 0.45 to 0.74 (median of 0.65). The large variations in the Cr# in the Cr-spinel of this district are due to the presence of both high-Al and high-Cr chromitites. High-Cr chromitites correspond to those from Caridad, Guarina, Monte Bueno, Tibera, and Albertina deposits (Fig. 1c) with Cr# ranging from 0.60 to 0.76 (median value of 0.66), and Mg# from 0.45 to 0.73 (median value of 0.64). Conversely, high-Al chromitites are related with Rupertina, Cernícalo, Negro Viejo, and Demajagua (Fig. 1c), with Cr# ranging from 0.46 to 0.65 (median value of 0.57) and Mg# from 0.60 to 0.74 (median value of 0.67). The minor and trace element composition ($n=60$; ESM 1 Fig. 3) shows contents of: 631–1062 ppm V (median of 836 ppm), up to 7 ppm Sc (median of 5 ppm), 27–49 ppm Ga (median of 44 ppm), 533–1747 ppm Ti (median of 994 ppm), 602–2343 ppm Ni (median of 1448 ppm), 584–918 ppm Zn (median of 717 ppm), 224–358 ppm Co (median of 253 ppm), and 1216–1926 ppm Mn (median of 1471 ppm).

Cr-spinel from Dunites and Harzburgites

Cr-spinel composition from dunites surrounding high-Cr chromitites ($n=35$; Figs. 5c and 6c and ESM 1 Fig. 2c) has Cr# varying from 0.65 to 0.80 (median of 0.72) and Mg# from 0.35 to 0.54 (median of 0.48). Conversely, Cr-spinel composition from dunites surrounding high-Al chromitites ($n=54$; Figs. 5c and 6c and ESM 1 Fig. 2c) has Cr# ranging from 0.57 to 0.63 (median of 0.58) and Mg# from 0.44 to 0.61 (median of 0.58).

Cr-spinel composition from harzburgites surrounding high-Cr chromitites ($n=82$; Figs. 5c and 6c and ESM 1 Fig. 2c) has Cr# that varies from 0.36 to 0.49 (median of 0.45) and Mg# from 0.60 to 0.67 (median of 0.64). On the other hand, Cr-spinel composition from harzburgites surrounding high-Al chromitites ($n=53$; Figs. 5c and 6c and ESM 1 Fig. 2c) has Cr# that ranges from 0.46 to 0.66 (median of 0.57) and Mg# from 0.47 to 0.60 (median of 0.57).

Moa-Baracoa district

Cr-spinel from chromitites

Moa-Baracoa chromitites ($n=696$; Figs. 5d and 6d and ESM 1 Fig. 2d) are classified as high-Al because their Cr-spinel has Cr# that vary between 0.41 and 0.57 (median of 0.46), while the Mg# range from 0.44 to 0.81 (median of 0.71). Minor and trace element composition ($n=56$; ESM 1 Fig. 3) shows contents of 939–1274 ppm V (median of 1183 ppm), 1–6 ppm Sc (median of 3 ppm), 43–68 ppm Ga (median of 58 ppm), 509–2251 ppm Ti (median of 1637 ppm), 1155–1855 ppm Ni (median of 1592 ppm), 485–672 ppm Zn (median of 625 ppm), 191–257 ppm Co (median of 211 ppm), and 1121–1381 ppm Mn (median of 1273 ppm).

Cr-spinel from Dunites and Harzburgites

Major element composition of Cr-spinel ($n=60$; Figs. 5d and 6d and ESM 1 Fig. 2d) from Moa-Baracoa dunites have Cr# that ranges from 0.44 to 0.57 (median of 0.48), and Mg# from 0.50 to 0.67 (median of 0.59). Major element

composition of Cr-spinel ($n=105$; Figs. 5d and 6d and ESM 1 Fig. 2d) from Moa-Baracoa harzburgites have Cr# that vary from 0.45 to 0.65 (median of 0.55), and Mg# from 0.39 to 0.68 (median of 0.55).

Mineral chemistry of Cr-spinel-hosted inclusions

In this section, the chemistry of Cr-spinel hosted silicate inclusions (olivine, pyroxene, amphibole, mica) is presented (Table 2; ESM 2).

Olivine

The composition of olivine grains included in Cr-spinel (ESM 1 Fig. 5a and ESM 2) from Mayarí, Sagua de Tánamo and Moa-Baracoa chromitites ($n=33$) yields high forsterite [Fo = Mg/(Mg + Fe^{2+}) molar ratio] contents (0.95 to 0.97; MgO from 51.9 to 55.8 wt%). The NiO contents oscillate from 0.36 to 0.93 wt% (median content of 0.69 wt%), similar to those observed in other olivine inclusions from other worldwide chromitites (ESM 1 Fig. 5a).

Table 2 Composition of the silicate inclusions (minimum, maximum and median values) within Cr-spinel grains

	Olivine	Pyroxene	Amphibole	Mica
SiO_2	41.3–42.9 (42.1)	50.1–55.3 (53.2)	46.7–50.0 (48.0)	37.9–43.0 (40.6)
TiO_2	b.l.d.	0.09–1.02 (0.66)	0.26–0.76 (0.69)	b.l.d.-1.67
Al_2O_3	b.l.d.	1.07–3.98 (3.18)	8.27–9.77 (9.20)	14.5–16.0 (15.2)
Cr_2O_3	0.24–1.32 (0.45)	1.13–2.08 (1.45)	2.59–3.99 (3.28)	2.53–4.27 (3.06)
MgO	51.9–55.8 (53.7)	16.0-18.2 (16.7)	19.5–21.3 (20.0)	25.0–31.0 (25.8)
CaO	b.l.d. −0.10	20.4–23.9 (23.3)	11.7–12.8 (12.3)	0.20–0.48 (0.30)
FeOt	3.25–5.17 (4.26)	1.32–2.39 (2.18)	b.l.d.	0.95–1.38 (1.29)
NiO	0.36–0.93 (0.69)	n/a	n/a	n/a
Na_2O	n/a	0.38–1.29 (0.78)	2.29–3.20 (2.84)	0.16–3.83 (2.42)
K_2O	n/a	n/a	0.07–0.26 (0.10)	0.24–1.59 (0.74)
F	n/a	n/a	b.l.d. −0.31	b.l.d.
Cl	n/a	n/a	b.l.d. −0.12	b.l.d. −0.18
Fo (mol%)	0.95–0.97 (0.96)	-	-	-
Xwo	-	0.43–0.49 (0.48)	-	-
Xfs	-	0.04–0.06 (0.05)	-	-
Xen	-	0.46–0.52 (0.48)	-	-

Clinopyroxene

Clinopyroxene grains hosted within Cr-spinel (ESM 1 Fig. 5b and ESM 2) from Camagüey, Mayarí, and Moa-Baracoa chromitites ($n=14$) are classified as diopside, with compositions ranging from $En_{46}Fs_5Wo_{49}$ to $En_{52}Fs_5Wo_{43}$. The Mg# varies between 0.93 and 1, the Al_2O_3 from 1.07 to 3.98 wt%, and the TiO_2 from 0.09 to 1.02 wt%. Similar clinopyroxene compositions have been found in other high-Al chromitites from Sartohay, China (ESM 1 Fig. 5a).

Amphibole

Amphiboles (ESM 1 Fig. 5c and ESM 2) have only been found in Cr-spinel from Sagua de Tánamo and Mayarí chromitites ($n=19$) and have Mg# values between 0.96 and 1, Al_2O_3 contents between 8.27 and 9.77 wt%, CaO between 11.7 and 12.8 wt%, Na_2O between 2.29 and 3.20 wt%, and TiO_2 between 0.26 and 0.76 wt%. Amphiboles Si atoms per formula unit vary from 6.56 to 6.90. All amphiboles are catalogued, according to Hawthorne et al. (2012) classification, as Ca-amphiboles, mostly corresponding to edenite, and to a lesser extent, pargasite. Amphiboles are typically reported in Cr-spinel-hosted inclusions in other chromitites worldwide (Uysal et al. 2009; Ullah et al. 2020; Zhu and Zhu 2020), which also show similar edenite-pargasite compositions.

Mica

Micas have only been found in high-Cr chromitites from Sagua de Tánamo ($n=7$; ESM 1 Fig. 5d and ESM 2). They classify as Na-phlogopite (aspidolite-like) with Na# (Na / [Na + K]) values between 0.51 and 0.88, Mg# between 0.97 and 0.98, and Cl contents reaching up to 1837 ppm. Na-phlogopites, and their K-rich counterparts have also been reported in other high-Al and high-Cr chromitites (Uysal et al. 2009; Khedr and Arai 2016; Zhu and Zhu 2020).

Platinum-group elements

Bulk-rock PGE contents in chromitites (Cr-spinel vol% > 85) from the four studied districts (ESM 4) vary from 22 to 109 ppb in Camagüey (median of 57 ppb), from 95 to 1423 ppb in Mayarí (median of 227 ppb; Proenza et al. 1999 and Gervilla et al. 2005), from 18 to 224 ppb in the high-Al chromitites of Sagua de Tánamo (median of 106 ppb; Proenza et al. 1999 and Gervilla et al. 2005), from 198 to 3713 ppb in the high-Cr chromitites of Sagua de Tánamo (median of 652 ppb; Proenza et al. 1999 and Gervilla et al. 2005), and from 30 to 166 ppb in Moa Baracoa (median of 84 ppb; Proenza et al. 1999 and Gervilla et al. 2005). The IPGE (Os,

Ir, Ru) are more abundant than the PPGE (Pd, Pt, Rh) in all four districts, with median IPGE/PPGE ratios varying from 3.28 to 6.52.

Chondrite-normalized patterns (ESM 1 Fig. 6) show that high-Cr chromitite districts (Mayarí and high-Cr Sagua de Tánamo) are more enriched in PGE compared to their high-Al counterparts, and have positive slopes to flat lines from Os to Ru and negative slopes from Ru to Pd. Additionally, the more PPGE-depleted samples from these two districts show negative anomalies in Pt. High-Al chromitite districts (Camagüey, Moa-Baracoa, high-Al Sagua de Tánamo) show chondrite-normalized patterns with negative Ir anomalies between Os and Ru, followed by negative slopes from Ru to Pd. These results compare well with previous PGE data from high-Al and high-Cr chromitites worldwide (ESM 1 Fig. 6) that show enrichment in IPGE with respect to PPGE and that high-Cr chromitites have higher PGE contents than high-Al chromitites.

Calculated melts in equilibrium with the chromitites

Major elements (Al_2O_3 and TiO_2)

The composition of Cr-spinel has been widely used to estimate the nature of chromitite parental melts and to elucidate the tectonic environment of formation (i.e. Arai 1992; Melcher et al. 1997; Proenza et al. 1999; Pagé and Barnes 2009; Farré-de-Pablo et al. 2020; Zhu and Zhu 2020; Pujol-Solà et al. 2021; Bo et al. 2023). The premise behind using Cr-spinel chemistry as a petrogenetic tool is based on the immobility of trivalent (Cr, Al) and tetravalent (Ti) cations in Cr-spinel at sub-solidus temperatures due to the low diffusivity of these cations in olivine (Scowen et al. 1991; Roeder and Reynolds 1991). Experimental results based on spinel-melt equilibrium at 1 bar (Maurel and Maurel 1982) and on the analysis of melt inclusions trapped in Cr-spinel from volcanic rocks (Kamenetsky et al. 2001) have shown that there is a linear relationship between the Al_2O_3 and TiO_2 contents of Cr-spinel and the Al_2O_3 and TiO_2 contents of the Cr-spinel's parental melt. Several authors have later refined these correlations using different power law expressions that better fit the ever-increasing datasets (Rollinson et al. 2008; Zaccarini et al. 2011; Zhu and Zhu 2020).

To calculate the Al_2O_3 composition of the parental melts for the studied chromitite districts we used the experimentally obtained equations of Maurel and Maurel (1982) and compared the results with the expressions obtained by Zhu and Zhu (2020) based on the data from Kamenetsky et al. (2001) (ESM 5). The results (Fig. 7a) show that the Al_2O_3 content of melts in equilibrium with high-Cr chromitites (Mayarí and high-Cr Sagua de Tánamo chromitites) is low (median values of ~12–13 wt%), and that the variations between the two different equations used account for only ± 1 wt%. The Al_2O_3 content of melts in equilibrium with high-Al chromitites (Camagüey, Moa-Baracoa and some Sagua de Tánamo chromitites) is higher (median values of ~15–16 wt%) and the variations between the results obtained using the different expressions are less evident (< 1 wt%).

To estimate the TiO_2 contents of melts in equilibrium with high-Cr and high-Al chromitites (ESM 5), we have used the expressions from Kamenetsky et al. (2001) modified by Zhu and Zhu (2020). The estimated TiO_2 compositions of the melts in equilibrium (Fig. 7b) show that the high-Cr chromitites parental melts have lower TiO_2 contents (median values: 0.25 and 0.39 wt% for Mayarí and Sagua de Tánamo, respectively) compared to high-Al chromitites (median values: 0.74, 0.75, and 0.50 wt% for Camagüey, Moa-Baracoa, and Sagua de Tánamo, respectively).

Trace elements

Pagé and Barnes (2009) empirically obtained the partition coefficients for several minor and trace elements in accessory Cr-spinel from MORB and boninitic lavas. Using these partition coefficients, other authors, such as Zhou et al. (2014) and Chen et al. (2019) estimated the trace element composition for the magmas in equilibrium with high-Al or high-Cr chromitites. Following this approach, the estimated trace element composition of the magmas in equilibrium with the chromitites of the four studied districts has been calculated (ESM 1 Fig. 7 and ESM 5). Regardless of equilibrium with high-Cr or high-Al Cr-spinel, the calculated melts are very similar in composition, especially in Ni, Zn, Co, Mn, and remarkably, in Ga, an element typically much more abundant in high-Al Cr-spinel than in high-Cr Cr-spinel (ESM 1 Figs. 3 and 4; Zhou et al. 2014). In contrast, Ti and V do show differences in the different calculated melts, being more enriched in the parental melts for high-Al chromitites than those of high-Cr chromitites (ESM 1 Fig. 7).

Discussion

Chromitite-forming Cr-spinel chemistry and parental magma compositions

The composition of the Cr-spinel in the chromitites from the four studied districts is very diverse, with a compositional spectrum that occupies almost completely and continuously the field defined by Cr-spinel in ophiolitic chromitites (Fig. 5). In high-Al chromitites (Camagüey and Moa-Baracoa districts), the Cr-spinel composition plots within

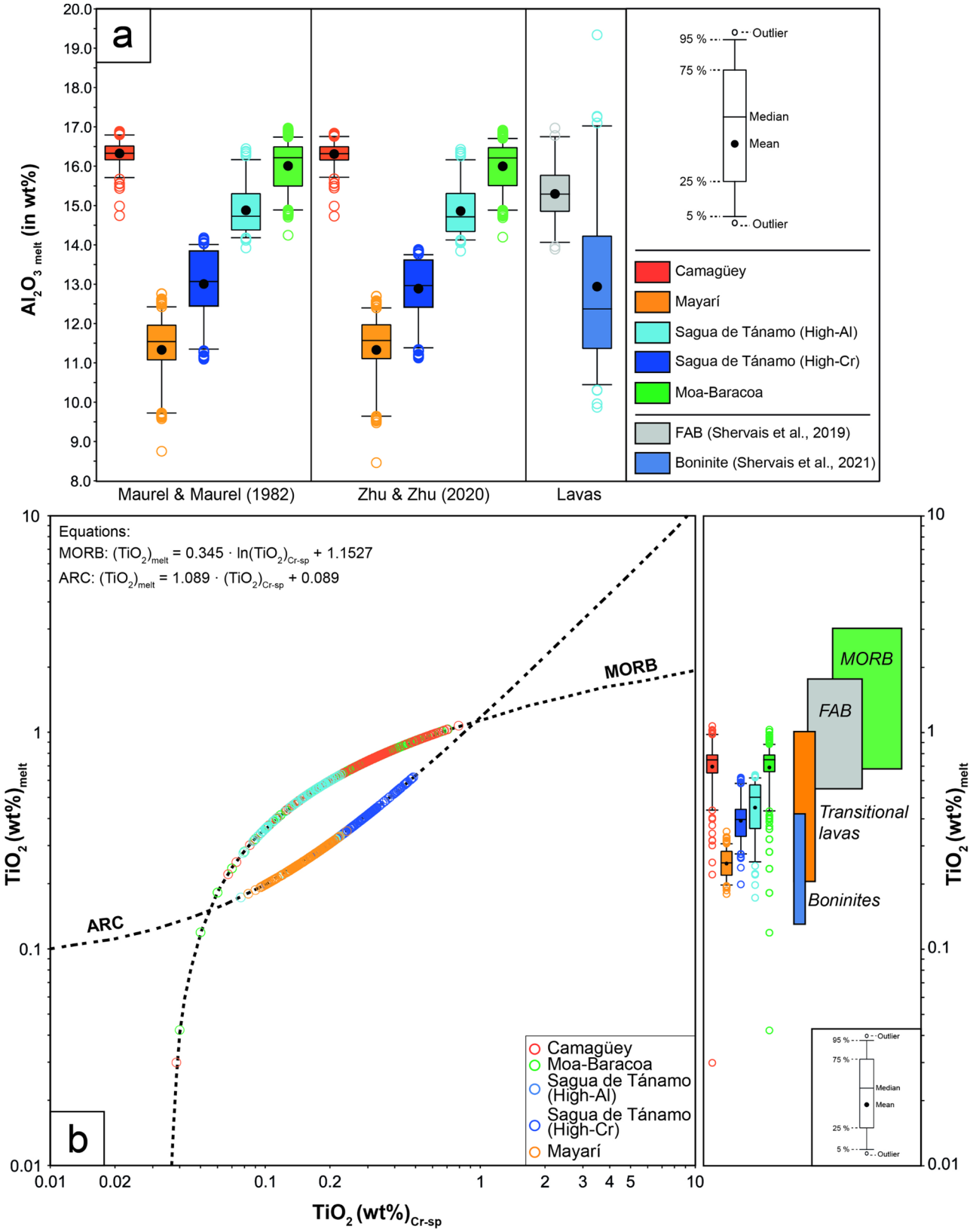
a
Al_2O_3 melt (in wt%)
Maurel & Maurel (1982)
Zhu & Zhu (2020)
Lavas
95 % Outlier
75 %
Median
Mean
25 %
5 % Outlier
Camagüey
Mayarí
Sagua de Tánamo (High-Al)
Sagua de Tánamo (High-Cr)
Moa-Baracoa
FAB (Shervais et al., 2019)
Boninite (Shervais et al., 2021)
Equations:
MORB: $(TiO_2)_{melt} = 0.345 \cdot \ln(TiO_2)_{Cr\text{-}sp} + 1.1527$
ARC: $(TiO_2)_{melt} = 1.089 \cdot (TiO_2)_{Cr\text{-}sp} + 0.089$
MORB
ARC
b
TiO_2 (wt%)melt
TiO_2 (wt%)Cr-sp
Camagüey
Moa-Baracoa
Sagua de Tánamo (High-Al)
Sagua de Tánamo (High-Cr)
Mayarí
MORB
FAB
Transitional lavas
Boninites

Fig. 7 Calculated composition of the melts in equilibrium with the chromitites from the four studied chromite districts. (**a**) Boxplot diagram showing the differences in the calculated Al_2O_3 (in wt %) of the melt considering the equations from Maurel and Maurel (1982), Zaccarini et al. (2011), and Zhu and Zhu (2020). Data is compared to the Al_2O_3 content of FABs (Shervais et al. 2019) and boninites (Shervais et al. 2021). (**b**) TiO_2 (Cr-spinel) vs. TiO_2 (melt) diagram. Equations are from Zhu and Zhu (2020). TiO_2 (melt) data is transformed to boxplots and compared to TiO_2 ranges of MORB, FABs, transitional FAB-boninitic lavas, and boninites based on data from Reagan et al. (2010), Shervais et al. (2019), and Ishizuka et al. (2020)

the field defined by Cr-spinel in MORB (Fig. 6 and ESM 1 Fig. 2; Arai 1992). The trace elements compositions normalized to accessory Cr-spinel in MORB (Pagé and Barnes 2009) are characterized by median flat patterns, thus resembling those from MORB (ESM 1 Fig. 4). However, some samples from Camagüey and Moa-Baracoa show strong variations in Ti, similar to what is observed in other high-Al chromitites (ESM 1 Fig. 4; Zhou et al. 2014; Chen et al. 2019; Pujol-Solà et al. 2022; Bo et al. 2023). Chromitites with anomalously high-Ti concentrations can be explained by fine-grained exsolutions of Ti-bearing minerals oriented following the (111) crystallographic planes of Cr-spinel, most likely rutile and/or ilmenite (Fig. 4l), which is a common process in Cr-spinel grains, as previously described by Augé (1987). On the contrary, low-Ti concentrations in high-Al Cr-spinel have been reported in the high-Al chromitites of Coto (Philippines) and interpreted as the result of melting of an uncommon SSZ fertile MORB mantle undergoing high-degrees of melt extraction in a two-step process (Zhang et al. 2023). In high-Cr chromitites (Mayarí district), the major element composition of Cr-spinel falls within the field defined by Cr-spinel in boninites (Fig. 6 and ESM 1 Fig. 2; Arai 1992). Their normalized trace element composition shows depletion in Ga, Ti, and Ni compared to Cr-spinel in MORB, which is characteristic of other high-Cr chromitites (ESM 1 Fig. 4; Pagé and Barnes 2009; Zhou et al. 2014; Chen et al. 2019).

The major element composition of Cr-spinel in the Sagua de Tánamo chromitites plots between the fields of accessory Cr-spinel in MORB and boninites (Fig. 6 and ESM 1 Fig. 2). In detail, it can be observed that high-Cr chromitites plot near or within the boninite field, whereas high-Al chromitites plot near the MORB field (Fig. 6d and ESM 1 Fig. 2d). This dichotomy is also observed in their trace elements composition (ESM 1 Fig. 3). On one hand, the behavior of trace elements of high-Al Cr-spinel resembles that of the Moa-Baracoa and Camagüey Cr-spinel, having higher concentrations of Ga, V, and Ni (ESM 1 Fig. 3) and MORB-normalized flat patterns (ESM 1 Fig. 4). On the other hand, high-Cr Cr-spinel of Sagua de Tánamo behaves similarly to the ones of Mayarí, with comparable MORB-normalized patterns and depleted Ga, V, and Ni contents (ESM 1 Figs. 3 and 4). In general, the Sagua de Tánamo Cr-spinel has major and trace element compositions that can be considered intermediate between the MORB-like high-Al compositions of Moa-Baracoa and Camagüey chromitites, and the boninite-like high-Cr compositions of Mayarí chromitites.

The estimated composition of the melts in equilibrium with each studied chromitite district has yielded a total of three distinctive types of parental magmas. Melts in equilibrium with high-Al chromitites of Camagüey and Moa-Baracoa have Al_2O_3 contents akin to MORB-like melts (Fig. 7; average Al_2O_3 14.7 wt%; Gale et al. 2013) and so are their trace elements MORB-normalized patterns which are generally flat (ESM 1 Fig. 4). However, their TiO_2 contents are too low (Fig. 7b) for a MORB-like melt (average TiO_2 1.68 wt%; Gale et al. 2013). The low Ti content of MORB-like melts, plus their estimated low Ti/V ratios (ESM 1 Fig. 7; median of 19.7) are however characteristic of forearc basalts (FAB; Reagan et al. 2010; Shervais et al. 2019) produced at the early stages of subduction-initiation. On the contrary, the high-Cr chromitites of Mayarí have low Al_2O_3 and TiO_2 contents (Fig. 7), which are consistent with boninite-like melts (average Al_2O_3 and TiO_2 contents of 12.4 and 0.27 wt%, respectively; Shervais et al. 2021; Fig. 7). Furthermore, their calculated MORB-normalized trace element patterns (ESM 1 Fig. 7) mimic the patterns of boninites (Li et al. 2019), which are characteristic of fluid-enhanced melting of the depleted suprasubduction zone mantle wedge during subduction-inititation (Shervais et al. 2021). Finally, the estimated melt compositions for the Sagua de Tánamo chromitites show that the chromitites of this district have parental melts ranging from FAB to boninitic compositions. High-Al chromitites have equilibrium melts resembling FAB-like melts due to their Al_2O_3 and TiO_2 contents and low Ti/V ratios (median of 9.6), whereas high-Cr chromitites, whose Al_2O_3 and TiO_2 contents are low, would be in equilibrium with boninite-akin melts (Fig. 7 and ESM 1 Fig. 7).

Trends of Cr-spinel chemistry in the harzburgite-dunite-chromitite system: implications for exploration

Chromitite bodies are usually separated from the harzburgitic host by dunite envelopes ("dunite channel", Fig. 2), which are typically interpreted as ancient melt conduits produced by pyroxene dissolution in the host harzburgites due to focused transport of percolating melts (i.e. Kelemen et al. 1995; González-Jiménez et al. 2014). In the studied high-Cr and high-Al chromitite districts (excluding Sagua de Tánamo as it contains both types of chromitites), Cr-spinel from the associated harzburgites, dunites, and chromitites

show contrasted trends that may shed light on the earliest stages of suprasubduction arc magmatism (Fig. 8).

The Cr-spinel composition from the harzburgites close to the chromitite bodies is quite similar in both types of chromite (high-Al and high-Cr) districts (median Cr# ~0.60, Mg# ~0.55 and TiO_2 ~0.05 wt%), but accessory Cr-spinel in dunites and Cr-spinel in chromitites show remarkable differences (Fig. 8). Cr-spinel from the associated dunites and chromitites of high-Al districts show lower Cr# values compared to the accessory Cr-spinel in the harzburgites from the same district, while Cr-spinel from dunites and chromitites of high-Cr districts show higher Cr# compared to their harzburgite counterparts. According to Suhr et al. (2003), such chemical variations in accessory Cr-spinel in dunites and Cr-spinel in harzburgites cannot be accounted for a single melting event and, therefore, two distinctive melt compositions must be considered.

Morishita et al. (2011) observed that accessory Cr-spinel from dunites directly dredged from the Izu-Bonin-Mariana forearc show high Cr# (Cr# ~ 0.8) or medium Cr# (Cr# ~ 0.55) compositions. They interpreted that dunites with medium Cr# Cr-spinel were formed as melt conduits in which FAB-melts circulated during the early stages of subduction-initiation. On the contrary, dunites with high Cr# Cr-spinel were pointed to be formed later, in equilibrium with boninitic melts. Our data suggest that this interpretation can be extended to the chromitite bodies found within dunites, and that the dunite and chromitite Cr-spinel composition records well the type of melt that it interacted with.

Consequently, accessory Cr-spinel composition of the peridotites surrounding chromitites can be used as tools to predict the composition of ophiolitic chromitites during exploration campaigns. Systematically, our study revealed how the accessory Cr-spinel composition from peridotites (dunites and harzburgites) hosting the chromitite bodies exhibit contrasted trends based on the composition of the chromitites. Cr-spinel from dunites associated with high-Al chromite deposits (refractory grade) have lower Cr# values compared to the accessory Cr-spinel from the associated harzburgites. On the contrary, Cr-spinel from dunites of high-Cr chromite deposits (metallurgical grade) show higher Cr# compared to the accessory Cr-spinel from the host harzburgites. Despite chromitites are spatially and genetically linked to dunites, dunites do not necessarily need to be found

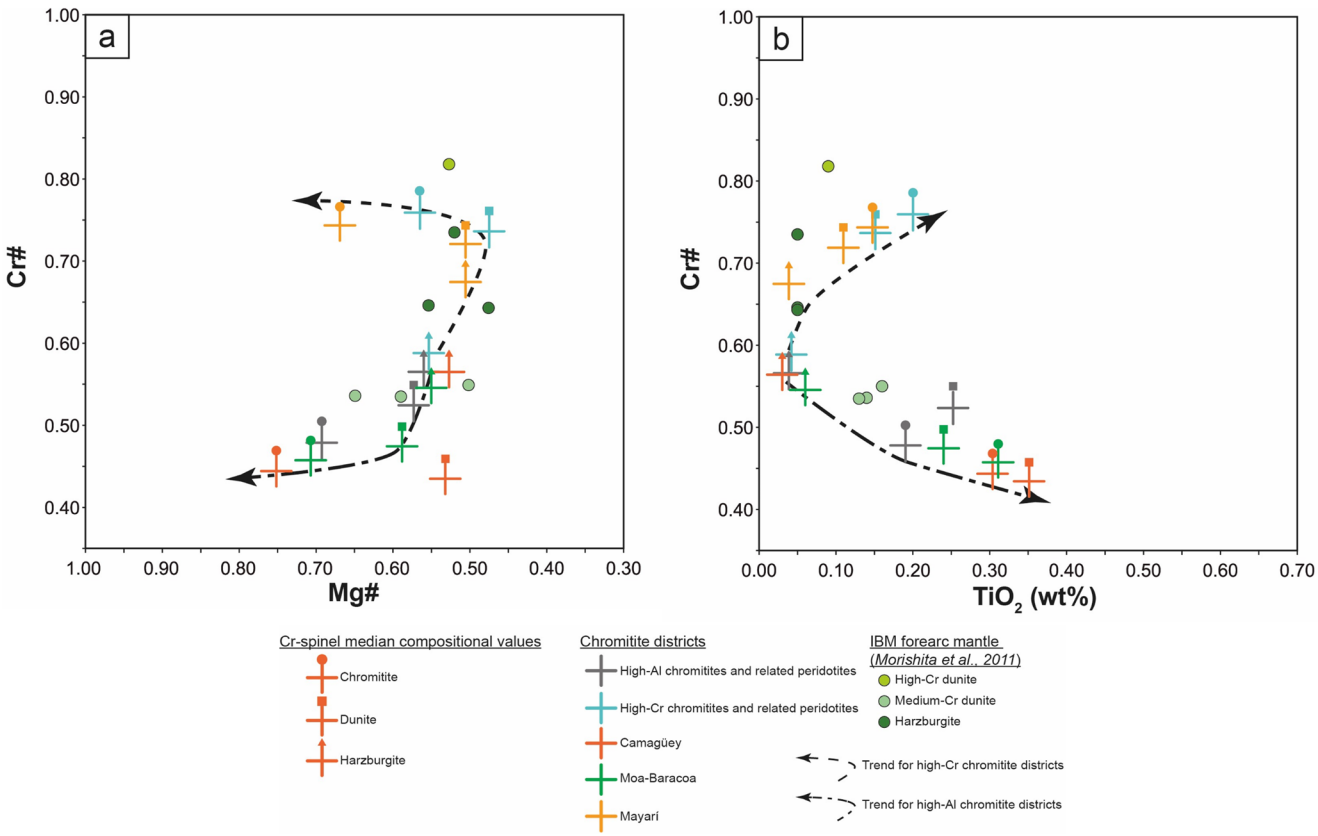

Fig. 8 Mg# vs. Cr# and TiO_2 (wt %) vs. Cr# diagrams showing opposite compositional trends for accessory Cr-spinel in harzburgites and dunites and Cr-spinel from chromitites from high-Cr (light blue) and high-Al (dark blue) chromitites from the different studied chromite districts. Data is compared to peridotites dredged from the IBM forearc (Morishita et al. 2011) and Cr-spinel in chromitites and related peridotites from other worldwide high-Al (Zhou et al. 2001b, 2014; Chen et al. 2019; Bo et al. 2023; Zhang et al. 2023) and high-Cr (Zhou et al. 1996, 2014; Xiong et al. 2015; Chen et al. 2019; Zhang et al. 2020) chromite districts

near any chromite ore body (Mosier et al. 2012). Therefore, in exploration campaigns of chromite deposits in ophiolitic sequences, the study of the mineral chemistry of accessory Cr-spinel in dunite is critical, as it sheds light on which kind of possible chromitites will eventually be found (high-Al and/or high-Cr). Moreover, the composition in major and trace elements of accessory Cr-spinel from dunites hosting or not chromite bodies is very similar (Proenza et al. 1999; Marchesi et al. 2006), and therefore, accessory Cr-spinel in dunites can be used as a proxy to estimate the composition of chromitites during exploration campaigns.

Petrogenetic implications from the PGE signature

Mantle peridotites typically contain disseminated base metal sulfides and platinum-group minerals (PGM), which are the ultimate responsible for controlling the distribution of PGE in the upper mantle (O'Driscoll and González-Jiménez 2016 and references therein). PGEs are divided into two groups, the IPGE and the PPGE, whose main difference resides in the fact that IPGE are more refractory than PPGE during partial melting (Barnes et al. 1985). Thus, during partial melting of mantle peridotites, the PPGE are transferred to the basaltic melts, whereas the IPGE stay trapped in the mantle residue (Bockrath et al. 2004). Therefore, the degree of partial melting reached in the mantle determines the extraction of PGEs (the higher the degree of partial melting, the higher the PGEs extraction from the mantle sources), and the differentiation between IPGEs and PPGEs from their mantle sources into the melts. Consequently, the PGEs signature of chromitites can shed light on the magmatic processes that led to their crystallization.

The chromitites from the four studied districts (ESM 1 Fig. 6) show how high-Cr chromitites have higher PGE contents (median of 246 ppb) and IPGE/PPGE ratios (median of 6.33) than the high-Al ones (median PGE contents of 79 ppb; median IPGE/PPGE ratio of 3.59) (ESM 1 Fig. 8). These characteristics are also observed in high-Cr chromitites (median PGE contents of 212 ppb; median IPGE/PPGE ratio of 6.27) and high-Al (median PGE contents of 70 ppb; median IPGE/PPGE ratio of 3.78) from around the world (ESM 1 Fig. 6).

Chondrite-normalized PGE patterns show that the main difference between high-Cr and high-Al chromitites reside in their IPGE contents, as both types of chromitites have similar PPGE contents (ESM 1 Fig. 6). This difference is directly related to the degree of mantle partial melting, which is correlated with the nature of chromitite parental melts. High-Al chromitites crystallized from FAB-like melts, whose mantle partial melting degrees are between 7 and 15% on average (Shervais et al. 2019). On the contrary, high-Cr chromitites crystallized after boninite-like melts formed after higher degrees of partial melting (~25%) of an already refractory mantle where FAB-like melts were already extracted (Shervais et al. 2021).

Sagua de Tánamo high-Al and high-Cr chromitites were in equilibrium with FAB-like and boninite-like melts, respectively, likely registering the transition from FABs to boninite magmatism during the evolution of the early stages of intra-oceanic subduction-initiation. This progressive transition is also recorded in the PGE signature of their chromitites (ESM 1 Fig. 6). The high-Cr chromitites are more enriched in PGEs, and more specifically in IPGEs, pointing toward higher degrees of partial melting, coherent with boninitic magmatism, which allowed the extraction of IPGEs from the mantle residue that were not able to be removed after the FAB-like magmatism that previously led to the crystallization of high-Al chromitites.

Chromitites record the geodynamic evolution of an intra-oceanic suprasubduction zone during subduction-initiation

In eastern Cuba, FAB magmatism was firstly documented at the La Tinta mélange, represented by amphibolitized dikes of dolerites with FAB affinity with a metamorphic cooling age of 123.2 ± 2.2 Ma (Lázaro et al. 2016). Later, Rui et al. (2021) interpreted that the Moa-Baracoa harzburgites originated in a nascent forearc mantle and were later crosscut by gabbro sills and dikes that have been dated at 136.7 ± 1.8 Ma (Rui et al. 2022). Rui et al. (2022) suggested that at > 137 Ma the proto-Caribbean plate started subducting underneath the Caribbean plate, thus marking the birth of the Caribbean island arc. Subduction-initiation produced by the sinking and rollback of the proto-Caribbean plate triggered (i) the extension of the Caribbean plate and the subsequent formation of its forearc region, and (ii) the mantle upwelling over the subducting proto-Caribbean slab. In this context, FAB melts were produced by the decompression and subsequent partial melting of the ascending asthenospheric mantle, in a similar fashion to how FAB magmatism is interpreted in the well-documented suprasubduction zone of the Izu-Bonin-Mariana (IBM) subduction system in the western Pacific (e.g. Reagan et al. 2010, 2019; Shervais et al. 2019, 2021). In equilibrium with these melts, the high-Al chromitite districts of Moa-Baracoa and Camagüey originated (Fig. 9). These districts are in equilibrium with melts similar to MORB but with lower TiO_2 contents (Fig. 7b) and low Ti/V ratios (ESM 1 Fig. 7) characteristic of FAB melts (Reagan et al. 2010; Shervais et al. 2019).

With the evolution of the subduction process, the altered oceanic crust and sedimentary cover in the subducting slab gradually starts to dehydrate (Shervais et al. 2021). Thus, fluid-enhanced melting of the depleted suprasubduction

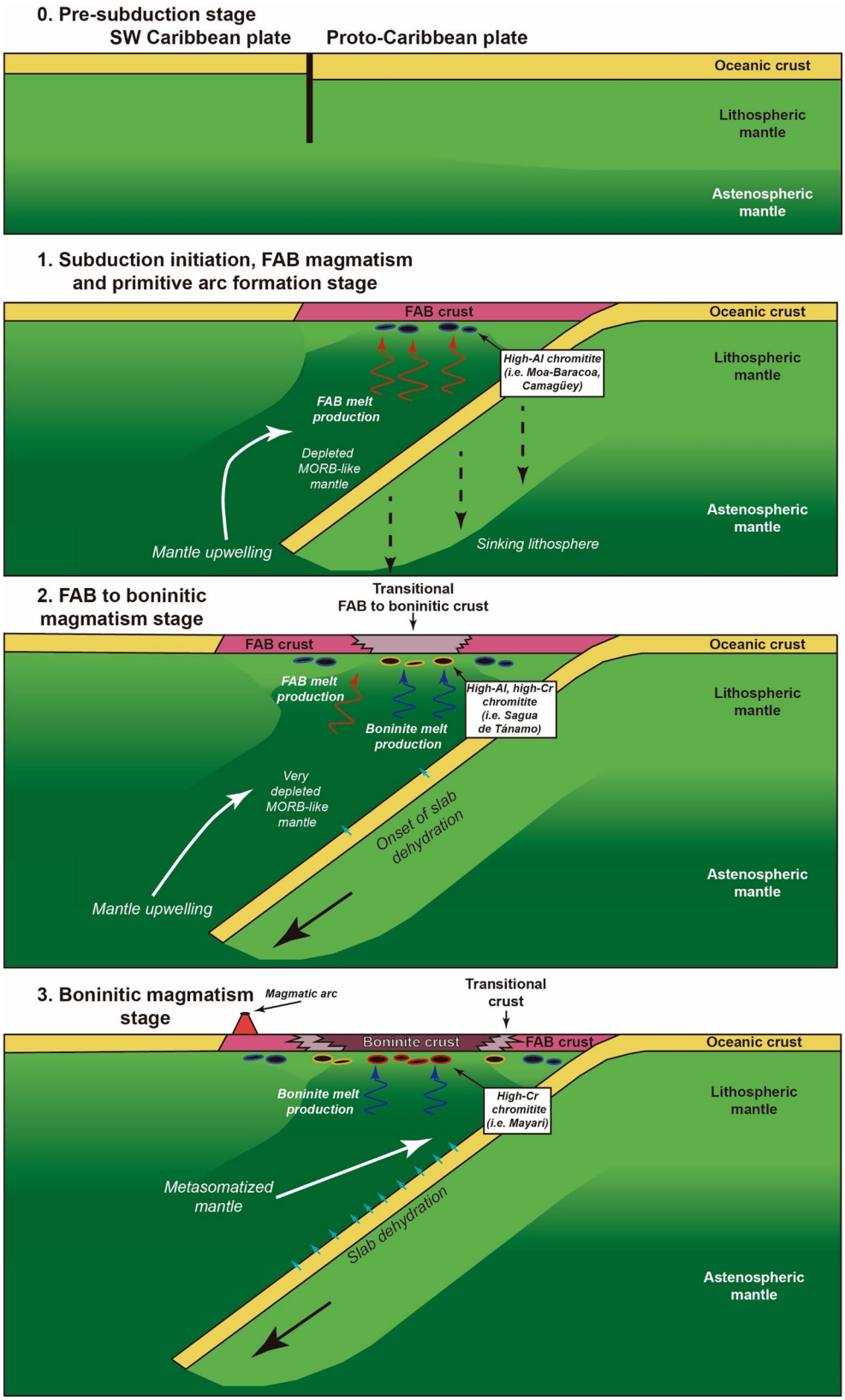

Fig. 9 Geodynamic evolution model for the studied chromite districts in a subduction-initiation geodynamic setting throughout three different stages. Stage 1 represents the onset of subduction-initiation and the formation of FAB melts resulting in the formation of high-Al chromitites from Camagüey and Moa-Baracoa districts. Stage 2 comprises the gradual shift from FAB to boninitic magmatism and the formation of the high-Al and later high-Cr chromitites from Sagua de Tánamo district. Stage 3 corresponds to more advanced stages of subduction-initiation with a continuous slab dehydration to generate boninitic melts that form the high-Cr chromitites from the Mayarí district

zone mantle wedge is produced, generating boninite magmas (Shervais et al. 2021). Boninite melts are characterized by high SiO_2 and MgO contents and low Al_2O_3 and TiO_2 contents that strongly differ from MORB/FAB magmas (e.g. Pearce and Reagan 2019; Shervais et al. 2021). The calculated composition of the melts in equilibrium with the high-Cr chromitites of Mayarí yields Al_2O_3 and TiO_2 contents that resemble those of boninites (Figs. 9 and 12). Furthermore, their calculated trace element composition mimics the trace elements patterns from boninites (ESM 1 Fig. 7). In addition, Cr-spinel from high-Cr chromitites contain abundant inclusions of hydrous silicates (amphibole and phlogopite; Fig. 4 and ESM 1 Fig. 5) that point towards the hydrated nature of the parental boninitic melt.

Nonetheless, the shift from FAB- to boninite-dominated melts during subduction-initiation is a gradual process produced continuously while the subducting slab sinks and progressively dehydrates (Reagan et al. 2010; Shervais et al. 2019, 2021). Consequently, magmatism originated during these intermediate stages should have a transitional nature between FABs and boninites (Reagan et al. 2010; Shervais et al. 2019, 2021; Chen et al. 2019). The generated melts will progressively evolve from a strong FAB-like component towards being controlled by an important slab-derived component. This steady shift of melt composition is observed in the chromitites from the Sagua de Tánamo district (Fig. 9). In this district, the high-Al chromitites, whose parental magmas have a major and trace element composition very similar to the high-Al chromitites from the Moa-Baracoa and Camagüey districts, record an important FAB-like component contribution in their composition, typical from earlier stages of subduction-initiation. On the contrary, the high-Cr chromitites of this district have melts in equilibrium with compositions that resemble the ones from the high-Cr chromitites of the Mayarí district, suggesting a stronger slab-derived component in their composition indicative of a more advanced stage of the subduction-initiation process.

Hence, when considering the different compositions observed in all four studied districts (Camagüey, Mayarí, Sagua de Tánamo, and Moa-Baracoa), it is possible to observe a bigger picture of the subduction-initiation process in an intra-oceanic setting (Fig. 9). The studied chromite districts allow tracing accurately the evolution of the subduction system, expected to have started at > 137 Ma, from the first FABs (stage 1 in Fig. 9), through the transitional magmatism (stage 2 in Fig. 9), to the more evolved boninitic stage (stage 3 in Fig. 9).

Conclusions

Chromitites from Camagüey and eastern Cuba record the complete magmatic evolution of an intra-oceanic subduction-initiation process. The high-Al chromitites from Camagüey and Moa-Baracoa districts were formed from FAB-like magmas, produced during the decompression and subsequent partial melting of the ascending asthenospheric mantle in the earliest stages of the intra-oceanic subduction of the proto-Caribbean lithosphere under the Caribbean lithosphere at > 137 Ma. Later, during more advanced stages of the subduction process, high-Cr chromitites from the Mayarí district crystallized in equilibrium with boninite-like magmas, produced by fluid-enhanced melting of the suprasubduction zone mantle due to the gradual dehydration onset of the subducting slab. The change from FAB-like to boninite-like magmatism during subduction-initiation is a gradual process produced continuously while the subducting slab sinks and progressively dehydrates. In this sense, Sagua de Tánamo district records well the steady shift of melt composition from FAB-like magmas, registered by its high-Al chromitites, towards boninite-like magmatism with a stronger slab-derived component, recorded by its high-Cr chromitites.

Additionally, accessory Cr-spinel composition of the ophiolitic peridotites can be used as an exploration tool and to anticipate the composition of ophiolitic chromitites. Whereas Cr-spinel from harzburgites is very similar in composition in either high-Al and high-Cr chromite districts, dunites Cr-spinel composition shows remarkable differences. Cr-spinel from dunites associated with high-Al chromite districts have lower Cr# values compared to the accessory Cr-spinel from the harzburgites. On the contrary, Cr-spinel from dunites of high-Cr chromite districts show higher Cr# compared to their Cr-spinel counterparts.

Supplementary Information The online version contains supplementary material available at https://doi.org/10.1007/s00126-025-01355-x.

Acknowledgements This research was financially supported by Spanish grant PID 2019-105625RB-C21 funded by MCIN/AEI/10.13039/501100011033 and by a "Ayudas predoctorales 2020" number PRE 2020–092140 PhD grant to DD-C by the Spanish Ministry of Science and Innovation. The help extended by the Empresa Geominera de Camagüey and Instituto de Geología y Paleontología / Servicio Geológico de Cuba during fieldwork are also gratefully acknowledged, as well as the technical support in EMPA sessions by Dr. Xavier Llovet. This paper has been produced within the framework of the MinResET (Mineral Resources for the Energy Transition) research group (2021-SGR-00239, Agència de Gestió d'Ajuts Universitaris i de Recerca de Catalunya). We are grateful to Associate Editor Frank Melcher, and two anonymous reviewers for their constructive suggestions that helped to improve the quality of the manuscript. Editor Bernd Lehmann is greatly appreciated for professional editorial handling of the manuscript.

Funding Open Access funding provided thanks to the CRUE-CSIC agreement with Springer Nature.

Declarations

Conflict of interest The authors have no competing interests to declare that are relevant to the content of this article.

References

Arai S (1992) Chemistry of chromian spinel in volcanic rocks as a potential guide to magma chemistry. Mineral Mag 56:173–184

Arai S (1997) Control of Wall-rock composition on the formation of podiform chromitites as a result of magma/peridotite interaction. Resour Geol 47:177–187

Arai S, Miura M (2016) Formation and modification of chromitites in the mantle. Lithos 264:277–295

Augé T (1987) Chromite deposits in the Northern Oman ophiolite: mineralogical constraints. Miner Deposita 22:1–10

Barnes SJ, Naldrett AJ, Gorton MP (1985) The origin of the fractionation of platinum-group elements in terrestrial magmas. Chem Geol 53:303–323

Blanco-Quintero IF, Proenza JA, García-Casco A, Tauler E, Galí S (2011) Serpentinites and serpentinites within a fossil subduction channel: La Corea mélange, Eastern Cuba. Geologica Acta 9:389–405

Bo RZ, Diley Y, Nasir S, Wu WW, Cai PJ, Lu YX, Lian DY, Yang JS (2023) Mineral and whole-rock geochemistry of high-Al podiform chromitites in the Fizh Massif of the Cretaceous Oman ophiolite: origin of hydrous N-MORB melts in a nascent forearc setting. J Geol Soc 180:jgs2023-047

Bockrath C, Ballhaus C, Holzheid A (2004) Fractionation of the platinum-group-elements during mantle melting. Science 305:1951–1953

Bonavia FF, Diella V, Ferrario A (1993) Precambrian podiform chromitites from Kenticha hill, Southern Ethiopia. Econ Geol 88:198–202

Burton J (2022) U.S. Geological Survey Releases 2022 List of Critical Minerals. https://www.usgs.gov/news/national-news-release/us-geological-survey-releases-2022-list-critical-minerals. Accessed 25th July 2024.

Chen C, Su BX, Xiao Y, Pang KN, Robinson PT, Uysal I, Lin W, Qin KZ, Avci E, Kapsiotis A (2019) Intermediate chromitite in Kızıldağ ophiolite (SE Turkey) formed during subduction-initiation in Neo-Tethys. Ore Geol Rev 104:88–100

Farré-de-Pablo J, Proenza JA, González-Jiménez JM, Aiglsperger T, Garcia-Casco A, Escuder-Viruete J, Colás V, Longo F (2020) Ophiolite hosted chromitite formed by supra-subduction zone peridotite–plume interaction. Geosci Front 11:2083–2102

Flint DE, Albear JF, Guild PW (1948) Geology and chromite deposits of the Camagüey District, Camagüey Province, Cuba. U.S. Geol Survey Bull 954:39–63

Gale A, Dalton CA, Langmuir CH, Su Y, Schilling JG (2013) The mean composition of ocean ridge basalts. Geochem Geophys Geosyst 14:489–518

García-Casco A, Iturralde-Vinent MA, Pindell J (2008) Latest Cretaceous collision/accretion between the Caribbean plate and Caribeana: origin of metamorphic terranes in the Greater Antilles. Int Geol Rev 50:781–809. https://www.tandfonline.com/doi/abs/10.2747/0020-6814.50.9.781

Garcia-Casco A, Torres-Roldán RL, Iturralde-Vinent MA, Millán G, Núñez-Cambra K, Lázaro C, Rodríguez Vega A (2006) High pressure metamorphism of ophiolites in Cuba. Geologica Acta 4:63–88

Gervilla F, Proenza JA, Frei R, González-Jiménez JM, Garrido CJ, Melgarejo JC, Meibom A, Díaz-Martínez R, Lavaut W (2005) Distribution of platinum-group elements and Os isotopes in chromite ores from Mayarí-Baracoa ophiolitic belt (eastern Cuba). Contrib Miner Petrol 150:589–607

González-Jiménez JM, Proenza JA, Gervilla F, Melgarejo JC, Blanco-Moreno JA, Ruiz-Sánchez R, Griffin WL (2011) High-Cr and high-Al chromitites from the Sagua de Tánamo district, Mayarí-Cristal ophiolitic Massif (eastern Cuba): constraints on their origin from mineralogy and geochemistry of chromian spinel and platinum-group elements. Lithos 125:101–121

González-Jiménez JM, Griffin WL, Proenza JA, Gervilla F, O'Reilly SY, Akbulut M, Pearson NJ, Arai S (2014) Chromitites in ophiolites: how, where, when, why? Part II. The crystallization of chromitites. Lithos 189:140–158

González-Jiménez JM, Locmelis M, Belousova E, Griffin WL, Gervilla F, Kerestedjian TN, O'Reilly SY, Pearson NJ, Sergeeva I (2015) Genesis and tectonic implications of podiform chromitites in the metamorphosed ultramafic Massif of dobromirtsi (Bulgaria). Gondwana Res 27:555–574

González-Pontón R (2009) Cromo Camagüey (proyecto de colaboración con el ALBA). Tercera Convención Cubana de Ciencias de la Tierra: La Habana, Cuba, Sociedad Cubana de Geología, memorias en CD-ROM, ISBN 978-959-7117-19-3

Guild PW (1947) Petrology and structure of the Moa chromite district, Oriente Province, Cuba. Eos, transactions. Am Geophys Union 28:218–246

Gupta V, Biswas T, Ganesan K (2016) Critical non-fuel mineral resources for India's manufacturing sector a vision for 2030. Council on energy, environment and water. CEEW) and Department of Science & Technology, Government of India

Hawthorne FC, Oberti R, Harlow GE, Maresch WV, Martin RF, Schumacher JC, Welch MD (2012) Nomenclature of the amphibole supergroup. Am Mineral 97:2031–2048

Henares S, González-Jiménez JM, Gervilla F, Proenza JA, Chang-Rodríguez A, González-Pontón RB (2010) Las cromititas Del Complejo Ofiolítico de Camagüey, Cuba: Un Ejemplo de Cromitas Ricas En al. Boletín De La Sociedad Geológica Mexicana 62:173–185

Instituto de Geología y Paleontología (1985) Hoja 22, mapa geológico de Camagüey, escala 1:250.000

Ishizuka O, Taylor RN, Umino S, Kanayama K (2020) Geochemical evolution of Arc and slab following Subduction-initiation: a record from the Bonin Islands, Japan. J Petrol 61:egaa050

Iturralde-Vinent MA (1996) Geología de las ofiolitas de Cuba. In Iturralde-Vinent, M.A., ed., Ofiolitas y arcos volcánicos de Cuba, IGCP Project 364, Special Contribution 1: 83–120

Iturralde-Vinent MA, Díaz-Otero C, Rodríguez-Vega A, Díaz-Martínez R (2006) Tectonic implications of paleontologic dating of Cretaceous-Danian sections of Eastern Cuba. Geologica Acta 4:89–102

Iturralde-Vinent MA, Garcia-Casco A, Rojas-Agramonte Y, Proenza JA, Murphy JB, Stern RJ (2016) The geology of Cuba: a brief overview and synthesis. GSA Today (Geological Soc America) 26:4–10

Kamenetsky VS, Crawford AJ, Meefre S (2001) Factors controlling chemistry of magmatic spinel: an empirical study of associated Olivine, Cr-spinel and melt inclusions from primitive rocks. J Petrol 42:655–671

Kelemen PB, Shimizu N, Salters VJM (1995) Extraction of mid-ocean ridge basalt from the upwelling mantle by focused flow of melt in Dunite channel. Nature 375:747–753

Khedr MZ, Arai S (2016) Chemical variations of mineral inclusions in neoproterozoic high-Cr chromitites from Egypt: evidence of fluids during chromitite genesis. Lithos 240–243:309–326

Lázaro C, Blanco-Quintero IF, Proenza JA, Rojas-Agramonte Y, Neubauer F, Núñez-Cambra K, Garcia-Casco A (2016) Petrogenesis and 40Ar/39Ar dating of proto-forearc crust in the early cretaceous Caribbean Arc: the La Tinta mélange (eastern Cuba) and its Easterly correlation in Hispaniola. Int Geol Rev 58:1020–1040

Lewis JF, Draper G, Proenza JA, Espaillat J, Jiménez J (2006) Ophiolite-related ultramafic rocks (serpentinites) in the Caribbean region: a review of their occurrence, composition, origin, emplacement and nickel laterite soils. Geologica Acta 4:237–263

Li HY, Taylor RN, Prytulak J, Kirchenbaur M, Shervais JW, Ryan JG, Godard M, Reagan MK, Pearce JA (2019) Radiogenic isotopes document the start of subduction in the Western Pacific. Earth Planet Sci Lett 518:197–210

Marchesi C, Garrido CJ, Godard M, Proenza JA, Gervilla F, Blanco-Moreno J (2006) Petrogenesis of highly depleted peridotites and gabbroic rocks from the Mayarí-Baracoa ophiolitic belt (eastern Cuba). Contrib Miner Petrol 151:717–736

Marchesi C, Garrido CJ, Bosch D, Proenza JA, Gervilla F, Monié P, Rodríguez-Vega A (2007) Geochemistry of cretaceous magmatism in Eastern Cuba: recycling of North American continental sediments and implications for subduction Polarity in the greater Antilles Paleo-arc. J Petrol 48:1813–1840

Maurel C, Maurel P (1982) Étude expérimentale de La distribution de L'aluminium Entre Bain silicaté basique et Spinelle chromifère. Implications pétrogénétiques: teneur En Chrome des Spinelles. Bull MinÃ©ral 105:197–202

Melcher F, Grum W, Simon G, Thalhammer TV, Stumpfl EF (1997) Petrogenesis of the ophiolitic giant chromite deposits of Kempirsai, Kazakhstan: a study of solid and fluid inclusions in chromite. J Petrol 38:1419–1458

Morishita T, Tani K, Shukuno H, Harigane Y, Tamura A, Kumagai H, Hellenbrand E (2011) Diversity of melt conduits in the Izu-Bonin-Mariana forearc mantle: implications for the earliest stage of Arc magmatism. Geology 39:411–414

Mosier DL, Singer DA, Moring BC, Galloway JP (2012) Podiform chromite deposits—database and grade and tonnage models: U.S. Geological Survey Scientific Investigations Report 2012–5157

Murashko VI, Lavandero RM (1989) Chromite in the hyperbasite belt of Cuba. Int Geol Rev 31:90–99

Nakano J (2021) The geopolitics of critical minerals supply chains. Centre for Strategic & International Studies (CSIS)

Nelson CE, Proenza JA, Lewis JF, López-Kramer J (2011) The metallogenic evolution of the greater Antilles. Geologica Acta 9:229–264

O'Driscoll B, González-Jiménez JM (2016) Petrogenesis of the platinum-group minerals. Rev Mineral Geochem 81:489–578

Pagé P, Barnes SJ (2009) Using trace elements in chromites to constrain the origin of podiform chromitites in the Thetford mines ophiolite, Québec, Canada. Econ Geol 104:997–1018

Pearce JA, Reagan MK (2019) Identification, classification, and interpretation of boninites from anthropocene to eoarchean geologic record using Si-Mg-Ti systematics. Geosphere 15:1–30

Proenza JA, Díaz-Martínez R, Iriondo A, Marchesi C, Melgarejo JC, Gervilla F, Garrido CJ, Rodríguez-Vega A, Blanco-Moreno JA, Lozano-Santacruz R (2006) Primitive Cretaceous island-arc volcanic rocks in eastern Cuba: the Téneme Formation. Geologica Acta 4:103–121

Proenza JA, Gervilla F, Melgarejo JC, Bodinier JL (1999) Al-and Cr-rich chromitites from the Mayari-Baracoa ophiolitic belt (eastern Cuba); consequence of interaction between volatile-rich melts and peridotites in suprasubduction mantle. Econ Geol 94:547–566

Proenza JA, Gervilla F, Melgarejo JC, Vera O, Alfonso P, Fallick A (2001) Genesis of sulfide-rich chromite ores by the interaction between chromitite and pegmatitic olivine–norite dikes in the Potosí mine (Moa-Baracoa ophiolitic Massif, Eastern Cuba). Miner Deposita 36:658–669

Proenza JA, Zaccarini F, Lewis JF, Longo F, Garuti G (2007) Chromian spinel composition and the platinum-group minerals of the PGE-rich Loma Peguera chromitites, Loma caribe peridotite, Dominican Republic. Can Mineral 45:631–648

Proenza JA, González-Jiménez JM, Garcia-Casco A, Belousova E, Griffin WL, Talavera C, Rojas-Agramonte Y, Aiglsperger T, Navarro-Ciurana D, Pujol-Solà N, Gervilla F, O'Reilly SY, Jacob DE (2018) Cold plumes trigger contamination of oceanic mantle wedges with continental crust-derived sediments: evidence from chromitite Zircon grains of Eastern Cuban ophiolites. Geosci Front 9:1921–1936

Pujol-Solà N, Proenza JA, Garcia-Casco A, González-Jiménez JM, Román-Alpiste MJ, Garrido CJ, Melgarejo JC, Gervilla F, Llovet X (2020) Fe-Ti-Zr metasomatism in the oceanic mantle due to extreme differentiation of tholeiitic melts (Moa-Baracoa ophiolite, Cuba). Lithos 358:105420

Pujol-Solà N, Domínguez-Carretero D, Proenza JA, Haissen F, Ikenne M, González-Jiménez JM, Colás V, Maacha L, Garcia-Casco A (2021) The chromitites of the neoproterozoic Bou Azzer ophiolite (central Anti-Atlas, Morocco) revisited. Ore Geol Rev 134:104166

Pujol-Solà N, Proenza JA, González-Jiménez JM, Gervilla F, Melgarejo JC, Marchesi C, Garcia-Casco A (2022) Comments on the paper Ti-poor high-Al chromitites of the Moa-Baracoa ophiolitic Massif (eastern Cuba) formed in a nascent forearc mantle by Rui. [ore Geol Rev 104847] Ore Geol Reviews 148:105019

Pushcharovsky Y (1988) Mapa Geológico de La República de Cuba Escala 1:250000. Academias de Ciencias de Cuba y la URSS

Reagan MK, Ishizuka O, Stern RJ, Kelley KA, Ohara Y, Blichert-Toft J, Bloomer SH, Cash J, Fryer P, Hanan BB, Hickey-Vargas R, Ishii T, Kimura JI, Peate DW, Rowe MC, Woods M (2010) Forearc basalts and subduction-initiation in the Izu-Bonin-Mariana system. Geochemistry, Geophysics, Geosystems 11: Q03X12

Reagan MK, Heaton DE, Schmitz MD, Pearce JA, Shervais JW, Koppers AAP (2019) Forearc ages reveal extensive short-lived and rapid seafloor spreading following subduction-initiation. Earth Planet Sci Lett 506:520–529

Roeder PL, Reynolds I (1991) Crystallization of chromite and chromium solubility in basaltic melts. J Petrol 32:909–934

Rollinson HS (2008) The geochemistry of mantle chromitites from the Northern part of the Oman ophiolite: inferred parental melt compositions. Contrib Miner Petrol 156:273–288

Rui HC, Yang JS, Llanes-Castro AI, Zheng JP, Liu F, Valdes-Mariño Y, Wu W, Qiu T (2021) Highly refractory Harzburgites from the Moa-Baracoa ophiolitic Massif, Eastern Cuba: insights into forearc mantle melt-rock interactions. Lithos 404–405:106427

Rui HC, Yang JS, Zheng JP, Llanes-Castro AI, Liu F, Wu Y, Wu WW, Valdes-Mariño Y, Masoud AE (2022) Early cretaceous subduction-initiation of the proto-Caribbean plate: geochronological and geochemical evidence from Gabbros of the Moa-Baracoa ophiolitic Massif, Eastern Cuba. Lithos 418–419:106674

Scowen PAH, Roeder PL, Helz RT (1991) Reequilibration of chromite from Kilauea Iki lava lake, Hawaii. Contrib Miner Petrol 107:8–20

Semionov YL (1968) Yacimientos Cromiticos de Cuba. Revista Tecnológica 3:17–30

Shervais JW, Reagan M, Haugen E, Almeev RR, Pearce JA, Prytulak J, Ryan JG, Whattam SA, Godard M, Chapman T, Li H, Kurz W, Nelson WR, Heaton D, Kirchenbaur M, Shimizu K, Sakuyama T, Scott YL (2019) Magmatic response to subduction-initiation: part 1. Forearc basalts of the Izu-Bonin Arc from IODP expedition 352. Geochem Geophys Geosyst 20:314–338

Shervais JW, Reagan MK, Godard M, Prytulak J, Ryan JG, Pearce JA, Almeev RR, Li H, Haugen E, Chapman T, Kurz W, Nelson WR, Heaton DE, Kirchenbaur M, Shimizu K, Sakuyama T, Vetterm SK, Li Y, Whattam S (2021) Magmatic response to subduction-initiation, Part II: Boninites and related rocks of the Izu-Bonin Arc from IODP Expedition 352. Geochemistry, Geophysics, Geosystems 22: e2020GC009093

Suhr G, Hellebrand E, Snow JE, Seck HA, Hofmann AW (2003) Significance of large refractory Dunite bodies in the upper mantle of the Bay of Islands ophiolite. Geochem Geophys Geosyst 4:8605

Thayer TP (1942) Chrome resources of Cuba. U.S. Geological Surbey Bulletin, 935-A

Ullah Z, Shah MT, Siddiqui RH, Lian DY, Khan A (2020) Petrochemistry of High-Cr and High-Al chromitites occurrences of Dargai complex along indus suture zone, Northern Pakistan. Episodes 43:689–709

USGS (2024) United States geological survey, mineral commodity summaries. Reston, VA. U.S. Geological Survey

Uysal I, Tarkian M, Burhan-Sadiklar M, Zaccarini M, Meisel T, Garuti G, Heidrich S (2009) Petrology of Al- and Cr-rich ophiolitic chromitites from the mug˘la, SW Turkey: implications from composition of chromite, solid inclusions of platinum-group mineral, silicate, and base-metal mineral, and Os-isotope geochemistry. Contrib Miner Petrol 158:659–674

Uysal I, Kapsiotis A, Melih-Akmaz R, Saka S, Seitz HM (2018) The Guleman ophiolitic chromitites (SE Turkey) and their link to a compositionally evolving mantle source during subduction-initiation. Ore Geol Rev 93:98–113

van Hinsbergen DJJ, Iturralde-Vinent MA, van Geffen PWG, Garcia-Casco A, van Benthem S (2009) Structure of the accretionary Prism, and the evolution of the paleogene Northern Caribbean subduction zone in the region of Camagüey, Cuba. J Struct Geol 31:1130–1144

Wilson FH, Orris G, Gray F (2021) Preliminary geologic map of the Greater Antilles and the Virgin Islands. US Geological Survey, Open-File Report 2019-1036, p 50, 2 sheets, scales 1:2,500,000 and 1:300,000

Xiong F, Yang J, Robinson PT, Dilek Y, Milushi I, Xu X, Chen Y, Zhou W, Zhang Z, Lai S, Tian Y, Huang Z (2015) Petrology and geochemistry of high Cr# podiform chromitites of Bulqiza, Eastern Mirdita ophiolite (EMO), Albania. Ore Geol Rev 70:188–207

Zaccarini F, Garuti G, Proenza JA, Campos L, Thalhammer OAR, Aiglsperger T, Lewis JF (2011) Chromite and platinum group elements mineralization in the Santa Elena ultramafic nappe (Costa Rica): geodynamic implications. Geologica Acta 9:407–423

Zhang PF, Zhou MF, Yumul GP Jr (2020) Coexistence of high-Al and high-Cr chromite orebodies in the Acoje block of the Zambales ophiolite, Philippines: evidence for subduction-initiation. Ore Geol Rev 126:103739

Zhang B, Zoheir B, Zhang C, Mu X, Xu X, Qiu T, Xiong F (2023) Coexisting High-Al and High-Cr chromitites in the Dingqing ophiolite (SE Tibet): inferences to compositional heterogeneity in the Tethyan upper mantle. Minerals 13:1234

Zhou MF, Lewis J, Malpas J, Muñoz-Gómez N (2001a) The Mayari-Baracoa paired ophiolite belt, Eastern Cuba: implications for tectonic settings and Platinum-Group elemental mineralization. Int Geol Rev 43:494–507

Zhou MF, Robinson PT, Malpas J, Aitchinson J, Sun M, Bai WJ, Hu XF, Yang JS (2001b) Melt/mantle interaction and melt evolution in the Sartohay high-Al chromite deposits of the Dalabute ophiolite (NW China). J Asian Earth Sci 19:517–534

Zhou MF, Robinson PT, Malpas J, Li Z (1996) Podiform chromitites in the Luobusa ophiolite (Southern Tibet): implications for melt-rock interaction and chromite segregation in the upper mantle. J Petrol 57:3–21

Zhou MF, Robinson PT, Su BX, Gao JF, Li JW, Yang JS, Malpas J (2014) Compositions of chromite, associated minerals, and parental magmas of podiform chromite deposits: the role of slab contamination of asthenospheric melts in suprasubduction zone environments. Gondwana Res 26:262–283

Zhu Q, Zhu Y (2020) Chromitite genesis based on chrome-spinels and their inclusions in the Sartohay podiform chromitites in West Junggar of Northwest China. Ore Geol Rev 119:103401